

Research Article

A Global Sensitivity Analysis of Dynamic Loading and Route Selection Parameters on Network Performances

Charlotte Duruisseau  and Ludovic Leclercq 

Univ. Lyon, ENTPE, IFSTTAR, LICIT, F-69518, Lyon, France

Correspondence should be addressed to Ludovic Leclercq; ludovic.leclercq@entpe.fr

Received 26 March 2018; Revised 21 September 2018; Accepted 2 October 2018; Published 15 November 2018

Academic Editor: Giulio E. Cantarella

Copyright © 2018 Charlotte Duruisseau and Ludovic Leclercq. This is an open access article distributed under the Creative Commons Attribution License, which permits unrestricted use, distribution, and reproduction in any medium, provided the original work is properly cited.

We conduct a Global Sensitivity Analysis (GSA) of urban-scale network performances to parameters representing a wide range of realistic dynamic loadings, decomposed in a choice of OD matrix, routing alternatives, and paths flow distribution. A special attention is given to the route alternatives generation, where overlapping metrics and selection methods are introduced to reproduce a wide variety of paths sets configuration. Paths flow distributions are calculated based on different equilibrium criteria. Several sets of simulations are conducted and analyzed graphically and then with a variance-based GSA method so as to get insights on how much and in which conditions each network loading parameter influences network performances by itself or by interaction. Results notably reveal that the demand level is the most decisive parameter since low values simply lead to free-flow conditions with no influence of the other parameters, whereas higher values lead to a wide diversity of network states going from close to capacity but stable to gridlocked. While a nonnegligible amount of this disparity is explained by the demand pattern parameter, the number of paths per OD, their overlapping, and the equilibrium criterion of the paths flow distribution are still influential enough to maintain the network close to its optimal capacity or to prevent the network from fast collapse (gridlock). The highlighted connection between spatial and temporal heterogeneities of the network states explains the gridlocking phenomena. These extracted insights are very encouraging for operational implementations.

1. Introduction

Dynamic network loading (DNL) components play a crucial role when estimating a network performance by simulation. DNL is the combination of the OD matrix definition, the path selection process, and the calculation of paths flow distribution for each OD pair. The first component is clearly related to the scenario. The third one has been extensively studied in the dynamic traffic assignment (DTA) literature in connection with the definition of different network equilibriums (user equilibrium (UE), bounded rationality UE, stochastic UE, system optimum, etc.) [1–3]. However, the selection method that reduces the vast number of possible paths in a meshed network into a candidate set of paths has received less attention. In particular, to the authors' best knowledge, no Global Sensitivity Analysis (GSA) has been conducted to assess how such paths selection influences the network performance over a simulation.

Several methods were established to generate paths sets. The classical K-shortest path algorithm is widely implemented. Link penalty [4] and link elimination methods are popular heuristics proceeding iteratively on links manipulation after identifying a shortest path. Ben-Akiva et al. [5] proposed a labelling approach exploiting the multiple attributes of each link to select paths based on different generalized cost functions. Across experiences, the overlapping properties of paths have been identified as essential for selecting routes realistically. In our study, we choose to characterize paths sets between ODs based on overlapping criteria and we then introduce specific selection methods.

Sensitivity Analysis (SA) can be defined as the study of how the variations in the model outputs can be attributed to the variations in the model inputs [6]. All the SA conducted in traffic endeavored to study the supply, focusing on parameters of the car-following models or the network capacities, or aimed to assess the performance of methodologies.

A sensitivity analysis was conducted by Punzo and Ciuffo [7] to characterize how calibration parameters of a microscopic simulation model impact the induced traffic dynamics. The study tackled the computational complexity of calibration by drawing good practices in the task. It clarified the role of parameters and allowed to simplify its resolution by breaking the calibration problem into subproblems. Punzo and Ciuffo [8] used a variance-based technique for parameter estimation and calibration of Intelligent Driver Model and the Gipps' model. In 2013, Ciuffo et al. explored the methodology of using Gaussian Process Metamodels for sensitivity analysis of traffic estimation models through a case study on the Aimsun mesoscopic model. The proficiency of the methodology was assessed. Ciuffo et al. [9] implemented a GSA to simplify the calibration of the IDM car-following model within the traffic simulation model. Punzo et al. [10] presented an implementation of a variance-based sensitivity analysis (Sobol indices estimated with Monte Carlo method) to simplify microscopic traffic flow models on the car-following model. Ge and Menendez [11] introduced an improved approach for the sensitivity analysis of computationally expensive microscopic traffic models and conducted a case study of the Zurich network in VISSIM. Ge et al. [12–15] presented a comprehensive approach for the sensitivity analysis of high-dimensional and computationally expensive traffic simulation models, combining screening and metamodel-based methods.

Only few studies started to characterize the influence of demand parameters on simulated traffic conditions through a sensitivity analysis. Furthermore, the existing studies only examined some particular components of the demand.

Parzani et al. (2016) proposed a methodology to investigate the impacts of demand distribution at link level on aggregated network performances with NMFD. However, only one parameter at the time was changed to study the influence; the paths overlapping and network definitions showed limitations that we tackle in this paper; the analysis did not study the influence of the number of paths per OD or the equilibrium criterion applied with DTA. For dynamic OD demand estimation, Djukic et al. [16] performed a sensitivity analysis of traffic conditions to the OD demand distributions over time. The first order Sobol indices were estimated with RBD-FAST technique due to the high number of variables. However, the route choice set is precomputed in Aimsun and does not vary among simulations. Chen et al. [17] implemented a Global Sensitivity Analysis to assess the impact of traffic demand on road emissions, derived from average traffic flow of each link every 15 min. First and total order Sobol indices were estimated with Monte Carlo method after fitting a metamodel based on the obtained observations, run with a dynamic traffic assignment model and user equilibrium criterion. However, traffic demand variability was modelled with a temporal profile for each cluster of OD pairs, link capacities, and vehicle float characteristics. Tobin and Friesz [18] introduced an approach for the sensitivity analysis of equilibrium traffic assignment problems. By introducing an equivalent restricted problem to have the desired uniqueness properties, the derivatives of the equilibrium arc flows are drawn in

response to perturbations in the cost functions and the trip table.

In this paper, we perform a systemic study of the network loading parameters on the network performances. Each block of the network loading decomposition is represented by several parameters. Our goal is to explore the whole search space created by these parameters with a Global Sensitivity Analysis based on microscopic dynamic simulations. We aim to conduct our analysis at the scale of a city with a network that mimics an urban setting with a high number of possible paths. Although some studies addressed the question of some parameters' influence on traffic conditions, no work analyzed the demand in such a systemic way. Furthermore, we aim to bring value in how to represent the variety of possible network loadings. We introduce a methodology to create and characterize a wide variety of possible paths sets configurations. The final originality that this work wants to achieve is the way to analyze simulation outputs. Indeed, not only do we process classical indicators on final network states, but also we conduct a deeper investigation on how the network came to such a state by looking into some spatial and temporal heterogeneity factors. Notably, this analysis helped to differentiate the stable networks from the nonstable ones. In the end, we were able to identify which parameters are influent, how much, and in which cases, bringing insights on how to make the network more efficient or resilient.

The paper is organized as follows. Section 2 presents an overview of the materials and methods of the study, introducing the simulation settings with the definition of the network and the network loading parameters. A brief overview of the chosen output indicators and their analysis method is presented. Section 3 presents the results, primarily through a graphical analysis and then through a quantification process with the analysis of Sobol indices. Section 4 presents the conclusions and recommendations for future research.

2. Materials and Methods

2.1. Simulation Settings

2.1.1. Definition of the Network. In this study, we are considering a regular network that mimics a Manhattan town with a ring road; see Figure 1. This network corresponds to 14×14 2-way regular roads with speed limit 50 km/h and intersections controlled by traffic lights, functioning on a simple 2-phase signal-timing scheme. These roads delimit blocks that are grouped 9 by 9 to form 5×5 zones. The 2-way ring road with speed limit 90 km/h separates the central zones from the peripheral ones with which it has 12 interchanges. Each link flow follows a triangular fundamental diagram. Details on regular roads intersection or interchange can be found in Figures 17 and 18.

2.1.2. Definition of the Network Loading Parameters. Given the high computational time of input design and simulation, we restricted the possible values of each input variable to a small set corresponding to the most representative cases and only simulated a subset of their possible combination. In this chapter, we go over the choice and design of values for each input, representing a component of the network loading.

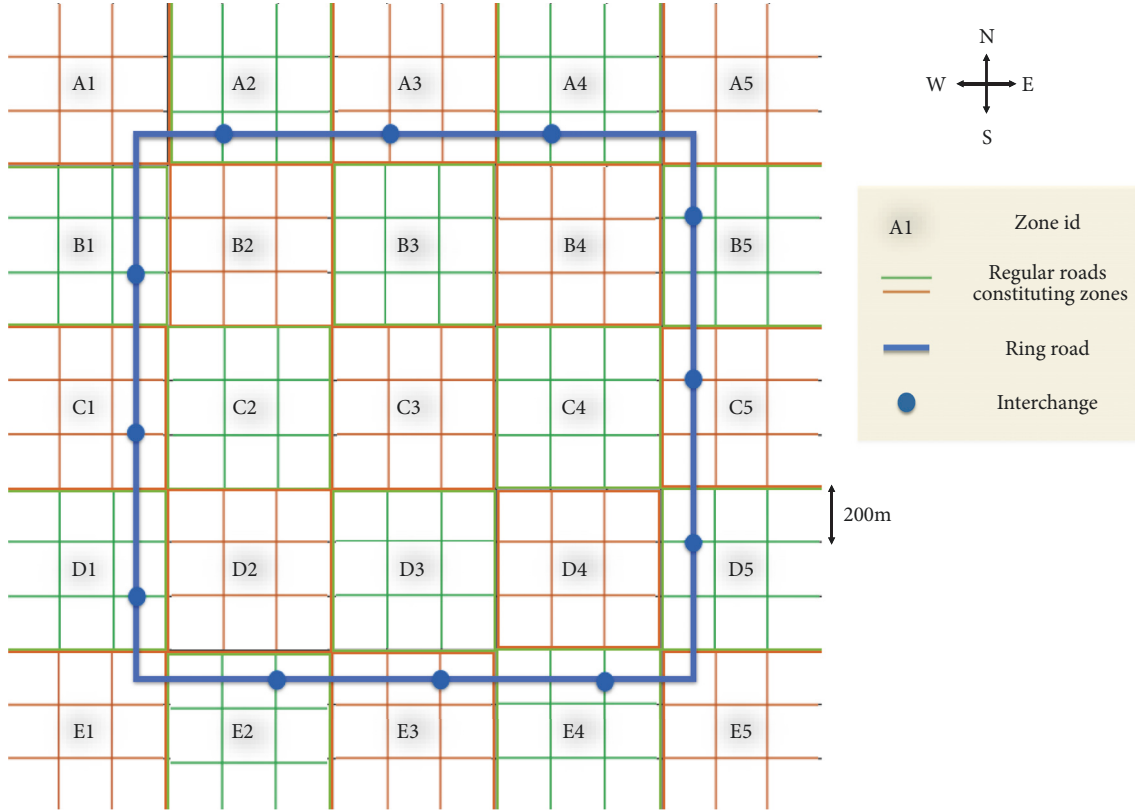


FIGURE 1: Support network: Manhattan town with ring road.

(1) OD Matrix

(i) *Distribution Demand Pattern.* As opposed to classical OD pair descriptions based on punctual network entries and exits, the OD matrix size is reduced to 25×25 by considering zone to zone demand patterns; see Figure 1. No flows are considered within zones; the diagonal of the OD matrix is null. For interzones flows, three demand distribution patterns were considered:

- (i) Uniform
- (ii) Exocentric (from periphery to center): could mimic urban rush hour in the morning
- (iii) Endocentric (from center to periphery): could mimic pick hour in the evening

These patterns were generated by two methods, leading to 6 possible values for the pattern variable. The first method starts from a uniform OD matrix where all cells are equal and simply increases the flows going from a peripheral zone to a centric one or vice versa so that the main moves represent 60% of the total flow.

The second method is based on a gravity model [19]. This distance-related distribution aims to produce more realistic OD flow distributions. For a uniform pattern, all zones have equal attraction and emission. The attractiveness of the central or peripheral zones was doubled for the other patterns, such that, in the end, any flow going to a central (resp. peripheral) zone is intensified.

(ii) *Total Demand Level.* The total demand is constant and uniformly distributed over the simulation time. Demand levels chosen for the study were calibrated on our network so as to reproduce a range of traffic conditions from free flow to saturated. Six levels of demand were considered in the study: level $k \times 25$ zones with k in vehicle per second unit and in the following set: $\{0.05, 0.10, 0.15, 0.20, 0.25, 0.30\}$.

(2) Dynamic Traffic Assignment

(i) Path Selection Method

Paths Definition. To overcome the high dimensionality of the problem, routes selection was defined between zone borders. We introduce the notion of junction points as the list of all network entry or exit points for each zone. The set of all possible paths from an origin to a destination zone gathers all possible paths between the related junction points. Upon simulation, vehicles are assigned a random position departure (resp. arrival) point within their origin (resp. destination) zone and are then automatically connected to the junction points related to their assigned path by the local shortest paths. For each OD, the selection method aims to narrow the set containing all possible paths to a candidate one, on which the demand OD flow is distributed. Figure 2 gives some illustrations of the paths definition process.

The paths selection method aims to select p shortest paths passing by regular roads, plus alternatives passing by the ring road for each OD. However, for some particular relative

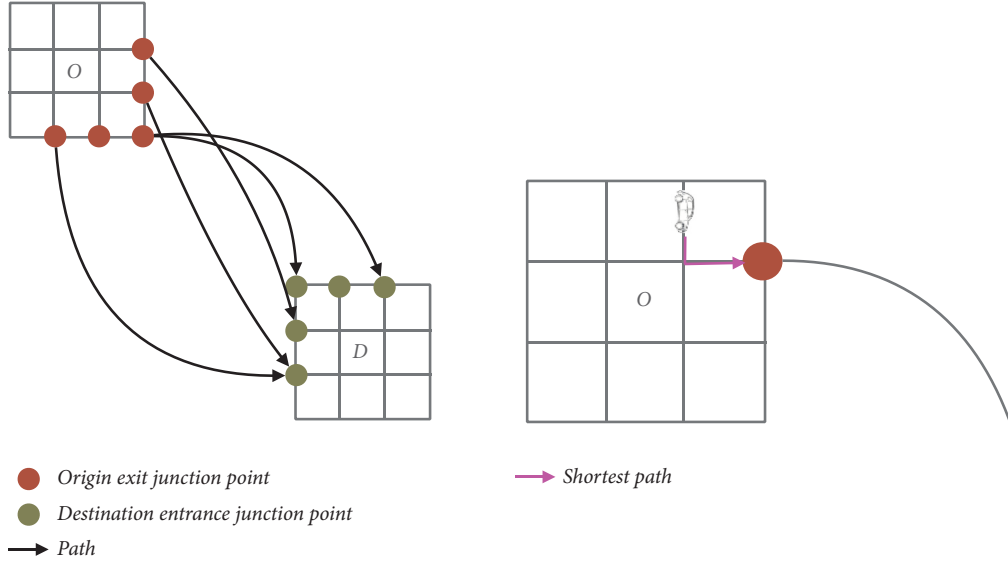


FIGURE 2: Schematic description of the paths definition.

positions of the origin and destination zones, less than p regular paths or no ring road paths were selected.

Selection on Ring Road. For OD zones far enough apart and close from interchanges, 2 paths taking the ring road (one in each direction) are selected such that they are the shortest alternative of their kind.

Selection on Regular Network. In a Manhattan network, paths only taking links in the direction of the destination are the shortest. As the combinatorial number of these shortest paths can be huge, we select, for each pair of junction points, an initial path set that homogeneously uses the available links in the right direction (the number of paths selected is proportional to the distance between the origin and destination). For an OD, the union of all these initial sets constitutes a candidate path set from which we will select the final paths with some overlapping criteria. Note that, for a given OD pair, not all junction points are necessarily connected after the selection process.

Selection Based on Local Overlapping. The chosen local overlapping indicator was inspired by the common factor CF_k defined by Cassetta et al. [20] and takes the following form:

$$LO_{ij} = \frac{L_{ij}}{\sqrt{L_i L_j}} \quad (1)$$

where LO_{ij} is the local overlapping score between paths i and j , L_{ij} is the shared length of paths i and j , and L_i (resp. L_j) is the length of i (resp. j). This pairwise overlapping measure is a real number between 0 and 1 and penalizes the difference of paths size.

For each OD, we calculated all pairwise overlapping scores generated by the candidate paths set. Then we proceeded 5 selections of p paths such that pairwise overlapping scores were either 0 (independent paths) or maximum or

within a range (one of the 3 intervals defined by $q1/3$ and $q2/3$ quantiles of the overlapping scores distribution). For the last method, paths were selected by a heuristic method with tolerance $2/3$ (or $1/2$ in some exceptional cases) due to the combinatorial difficulty of the thousands of possible selections.

Selection Based on Global Overlapping. Interactions between paths sets of distinct ODs are not taken into account in the above selection strategy based on local overlapping. Thus, this strategy aims to focus the path selection on the degree of overlapping at network level. Now, paths between OD pairs are selected all at once in function of the resulting global overlapping score.

We introduce a global overlapping indicator based on the idea to compare the paths distribution over the links to an ideal even distribution:

$$GO = \sum_{link\ i} (x_i - x^*)^2 \quad (2)$$

where GO is the global overlapping score, equal to the sum over all the network links of the squares of the gaps between x_i , the number of paths passing by the links i and x^* , an average number of paths by link. In practice, x^* is scaled for each p by performing 10000 random drawings of p paths per OD and calculating the average ratio of length between the $25 \times 24p$ drawn paths and the network links. For each p , the 4 levels of global overlapping were defined from the $q1/4$, $q1/2$, and $q3/4$ quantiles of the random drawings GO scores distribution.

(ii) Paths Flow Distribution. In this study, we apply classical dynamic traffic assignment principles. We mainly focus on the deterministic user equilibrium (UE) where travel times on all chosen paths for a given OD are equal. The UE is based on the Wardrop first principle [21]. We also consider the ideas of users' bounded rationality [22–25] that relax the

assumptions of the UE. In this framework, users look for “satisficing” paths instead of the ones that minimize their own travel time. The term “satisficing” was introduced by the original works of Simon and stands for the concatenation of the words “suffice” and “satisfy”. These ideas of bounded rationality were firstly introduced to the route choice context by Mahmassani et al. [26]. The authors introduced the concept of indifference bound ($\epsilon\%$), where users are satisfied if their route’s travel time is not superior to the minimal travel times of the OD pair by $\epsilon\%$. The network equilibrium then corresponds to the bounded rationality user equilibrium (BRUE) [27, 28]. A review paper about bounded rationality behavior applied to route choice is provided by Di [29]. In this paper, we consider the following values for ϵ : 10%, 20%, and 30%.

The network equilibria are solved considering the Method of Successive Averages (MSA) [30, 31]. More precisely, we are using the Smart MSA approach proposed in Sbayti et al. [32]. In each simulation, the set of possible paths is predefined for each OD pair and the same set is kept over the simulation time. Note that we are not using path discovery technics that may exist in some DTA algorithms because, in our study, we are monitoring the path overlapping that should then remain constant over a simulation. The final paths flow distribution corresponds to the final step of the Smart MSA algorithm, that is, after convergence. At each iteration step, this method considers the experimented travel time of the previous iteration step to determine the new candidate paths flow distribution. When convergence is reached, that is, when equilibrium conditions are met, the final paths flow distribution guaranties that, for all OD pairs, experimented travel times on the paths connecting the same OD pair are similar for UE or in the range of $\epsilon\%$ for BRUE. More precisely, we are using the relative gap function G_1 for DUE [32]:

$$G_1 = \frac{\sum_o \sum_d \sum_p n_p^{od} (T_p^{od} - T_{min}^{od})}{\sum_o \sum_d n_p^{od} T_{min}^{od}} \quad (3)$$

where T_{min}^{od} is the minimal experimented travel times for an OD pair od considering all paths, T_p^{od} is the current travel time on path p for OD pair od , and n_p^{od} is the number of users that are taking path p for OD pair od . G_1 corresponds to the average difference in time per user between the current path travel time and the minimal travel time for each OD. So, a perfect user equilibrium for all OD pairs means $G_1=0$. In practice, we have set G_1 equal to 5 s. All simulations that were not meeting these values were run again with more iterations. Only very few simulations were not able to converge after this second stage and were then disregarded.

We have extended this definition for BRUE considering that the reference travel time for each OD pair is no longer the minimum experimented travel time T_{min}^{od} but $(1 + \epsilon)T_{min}^{od}$. So, the gap function G_2 for BRUE is defined as

$$G_2 = \frac{\sum_o \sum_d \sum_p n_p^{od} \max(T_p^{od} - (1 + \epsilon)T_{min}^{od}, 0)}{\sum_o \sum_d n_p^{od} T_{min}^{od}} \quad (4)$$

Convergence was considered achieved when $G_2 = 5$ s. Again, we sometimes needed to increase the number of iterations to

reach convergence but all simulations converged in that latter case.

In this paper, we are going to consider two types of assignment period. The first one, called “static assignment,” is when a unique assignment period covers the whole simulation period. This means that paths flow distributions are calculated once for all during the simulation considering mean travel times over the full period. The second, called “dynamic assignment,” is when the paths flow distribution is updated every 20 minutes considering traffic conditions over such a time period. This permits to refresh the assignment discipline for all ODs when travel times are evolving during the simulation.

2.1.3. Simulator. Traffic dynamics are calculated by the Symuvia simulation tool developed by the LICIT laboratory. This dynamic and microscopic platform is founded on Newell’s car-following rule [33], which is the Lagrangian resolution of the LWR model [34] and includes most features (multiclass, lane-changing, intersections, etc.) required to simulate urban traffic.

In our study, each simulation lasted roughly between 30 minutes and 3 hours.

2.1.4. Outputs: Indicators of Network Performances. We simulated the demand conditions in the chosen network over 1h30 starting from an empty network state. Performance outputs were calculated on the 1-hour observation period, starting after a warm-up period of 20 minutes, ending 10 minutes before the end of the simulation time.

(i) **Global Indicators of Network State.** To characterize the network state, we looked at classical global indicators: Total Travel Time (TTT), Total Travel Distance (TTD), and Mean Speed = TTD/TTT, which really reflects the network’s quality of service.

(ii) **Network Heterogeneity.** To appreciate the heterogeneities in network performances, we looked at the following:

- (a) A **spatial heterogeneity factor**: the standard deviation of link mean speed (only nonempty links are taken into account) normalized by the network mean speed, over the last 20 minutes of the observation period to characterize final network states.
- (b) A **temporal heterogeneity factor**: the gridlock drop rate (GDR) was introduced during the analysis of simulation results. Details on its definition will be provided in the Graphical Analysis section.

2.1.5. Variance-Based Sensitivity Analysis: Estimation of Sobol Indices. The variance-based Sobol indices were chosen to perform our Global Sensitivity Analysis [35].

Each of the performance scalar outputs y (alternatively TTD, GDR, or SH) can be expressed as a function of the input parameters x_i (i between 1 and 5) of our problem. x_1 is the demand level, x_2 is the demand pattern, x_3 is the equilibrium criterion, x_4 is the overlapping level, and x_5 is the number of paths per OD. A Global Sensitivity Analysis based on Sobol

indices requires that input parameters be independent. In practice, it is always difficult to provide a formal proof of that but, in our case, we can consider that this assumption holds as there is no clear relationship between the 5 input variables we defined.

Let us note x as the vector of our input parameters x_i . In the following formulas explaining the construction of the Sobol indices, we are taking the example of TTD as the y output and note by f the function that relates TTD to the x_i .

The constitution of the Sobol indices relies on the Sobol-Hoeffding unique decomposition [36–38] of f :

$$\begin{aligned} TTD &= f(x) = \sum_{I \subseteq \{1, \dots, 5\}} f_I(x_I) \\ &= f_0 + \sum_{1 \leq i \leq 5} f_i(x_i) + \sum_{1 \leq i < j \leq 5} f_{i,j}(x_i, x_j) + \dots \end{aligned} \quad (5)$$

x_I and x_J are subvectors of x .

As the f_I satisfy

$$E(f_I(x_I) | x_J) = 0 \quad (6)$$

That is, they are orthogonal because of the independence between input parameters; the variance of f can be decomposed as

$$\text{var}(f(x)) = \sum_{I \subseteq \{1, \dots, 5\}} \text{var}(f_I(x_I)) \quad (7)$$

The Sobol indices represent the fraction of variance explained by the variables in I :

$$S_I = \frac{\text{var}(f_I(x_I))}{\text{var}(Y)} \quad (8)$$

The total Sobol indices [39, 40] represent the fraction of variance explained by each variable by itself or interaction effect with other variables:

$$S_I^T = \frac{\text{var}(\sum_{I \ni i} f_I(x_I))}{\text{var}(Y)} \quad (9)$$

In practice, calculating Sobol indices can be quite computationally expensive. Thus, we chose to perform simulations following a design of experiment containing 20% of the search space, selected by Latin Hypercube Sampling (LHS). For this operation, we used built-in functions in the R library DiceDesign to create a LHS in a 5-dimension unit cube and optimize the spread of the points with a Maximin algorithm and then transposed the created hypercube into our discrete domain (we only allowed a predefined set of values for each input parameter) by projecting the drawn coordinates on the lower bound of the unit subintervals of equal size. Then, we ran the simulations on these selected combinations of input parameters. Finally, for each output parameter, we fitted a Kriging metamodel [41] on our simulations' observations to estimate the above function expressing y in terms of the x_i . This metamodel allowed us to estimate Sobol indices with the Monte Carlo method [42, 43]. With this process, we estimated first order, second order, and total Sobol indices

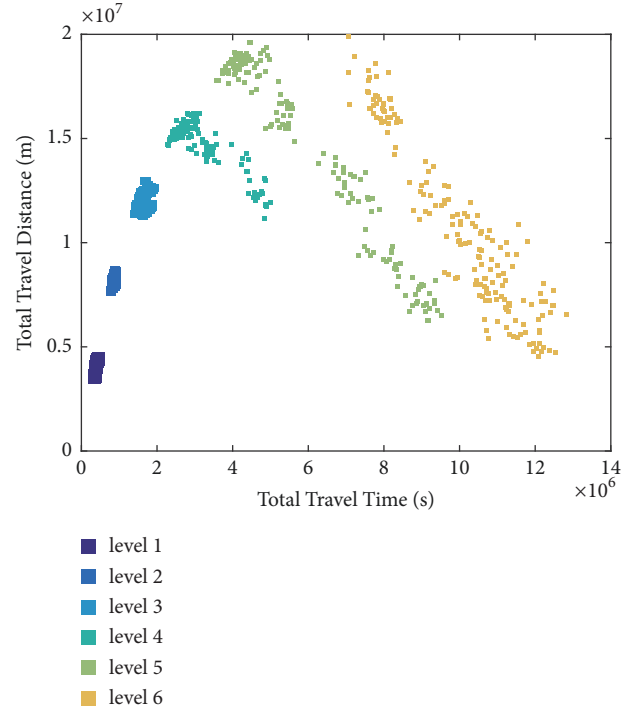


FIGURE 3: Final network states of 50 min simulations, colored by demand level.

for each performance indicator that we wanted to study. For these operations, we used the R library DiceKriging and Sensitivity. The Kriging metamodel parameters were estimated by Maximum Likelihood; the covariance structure used was Matérn 5/2; predictions were made with Universal Kriging. The coordinates of the calls to the metamodel followed a uniform distribution on each dimension.

3. Results

Two complementary phases of analysis were performed: first, the graphical analysis allows to identify which value(s) of the network loading parameters are associated with great or weak performances; then a quantitative analysis based on Sobol indices allows to quantify the proportions of performance variances due to each network loading parameter.

3.1. Graphical Analysis

3.1.1. Graphical Analysis of Results with Average Assignment Period. Figure 3 presents the final network states from a first set of 50-minute-length simulations in terms of TTD and TTT, colored by the level of demand applied. We immediately note the separation of performance scores by the demand level primer effect.

Each of the three lowest levels of demand (from level 1 to level 3) led its simulations to similar network performances after 50 minutes of simulation even though each single dot corresponds to an experience with different settings. We conclude that these simulations maintained free-flow conditions and experienced no influence of the network

loading variables on their TTD or TTT performance, apart from the demand level. This means that the demand pattern, the paths overlapping level, the number of paths per OD, and the flow equilibrium criterion do not change the final network state in free flow.

On the other hand, each of the three highest levels of demand presents networks experiencing a wide range of traffic states from saturation to heavy congestion: in addition to discrimination by level of demand, the simulations end with a variety of TTD and TTT performances. How do network loading parameters other than demand level play a role in the simulated network performance? Furthermore, congestion is known not to be a stable state at the network level. So, how would these network states evolve over time?

To answer these questions, we will first look into the progression of the network performances over time to highlight the associated dynamics. Precisely, for each of the three highest levels of demand, all simulations were run on a longer time interval of 90 minutes.

In Figure 4, each marker stands for a simulation state in terms of TTD and TTT. The graphs (a)&(b), (c)&(d), and (e)&(f), respectively, present the temporal evolution of simulations with demand levels 4, 5, and 6. On graphs (a)&(c)&(e), the state of each simulation is represented as every slot of 20 minutes, after a warm-up period of 20 minutes: the states evolve from blue, to orange, to green. On graphs (b)&(d)&(f), only a few selected simulations are plotted so as to highlight the time evolution of the related network states for each demand level.

We observe that some simulations keep a constant high value of TTD over the simulated time, while others have a TTD score decreasing at a simulation-specific rate towards zero. While the first case indicates maintained good network conditions and thus calls for a network stable state, the latter case indicates a network state worsening at a certain speed over time towards a state of gridlock. For longer simulated times, we suspect persistence of the stable states and convergence to gridlock for all other simulations.

While a high demand level of 5 or 6 systematically leads to low TTD over time, demand level 4 also allows slow transitions to gridlock and stable high network performances to happen: the demand level seems to be the primer responsible of possible network states evolutions.

The large spread of TTD scores with reasonable level 4 of demand indicates that a simulation's performance is highly influenced by the other loading metrics. Which parameters influence the rate of state deterioration or are even able to keep the network in a stable state? Let us focus on the simulation results with demand level 4 so as to clearly identify these effects.

We will sequentially study the influence of the remaining loading variables: demand pattern, equilibrium criterion, number of paths per OD, and local or global overlapping level.

Identification of Direct Effects of Loading Variables on TTD. In Figure 5(a) the simulations' final states are plotted (corresponding to the green markers for demand level 4 in the previous graphs) colored by demand pattern value. The table (Figure 5(b)) gives for each demand pattern the total

distance to travel implied in increasing order, as well as the corresponding TTD standard deviation. The "distance to travel" is the theoretical value of the total distance that would be travelled if every vehicle finished its trip by the end of the simulation. The TTD is the observed value of distance travelled during the simulation. Note that here the distance to travel is significantly higher than the TTD because we are analyzing congested scenarios where lots of vehicles are still queuing outside the network without having entered yet at the end of the simulation.

The demand pattern clearly segregates the simulations by performance level, showing an obvious direct effect. Furthermore, clusters made by the demand pattern parameter display various sprawl geometries. Classifying them by their TTD standard deviation score permits to distinguish 3 types of network states distributions:

Convex but spread, with a score ranging between 10^6 and 4×10^6 , groups "To Center," "Gravity to Center," and "To Edges" patterns

Bi-polar, with a score ranging above 4×10^6 , groups "Uniform" and "Gravity Uniform" patterns

Gathered and close, with a score ranging below 10^6 , groups the "Gravity to Edges" pattern.

Additionally, we shall note that this pattern classification is 98% correlated with the total distance to travel implied by each pattern. The distance to travel increases 7.5% from *convex but spread* to *bi-polar* to *gathered and very close* patterns. A higher distance to travel implies more vehicles simultaneously present on the network and thus worse traffic conditions. This may explain the observed difference of average performance between the patterns.

As shown in Figure 6, coloring the same TTD performances by the remaining assignment parameters does not reveal such a clear direct effect: points are not globally well separated by any color. However, if we focus on what separates TTD scores of a simulation set with the same demand pattern, that is, separations independent of this variable, we observe a dissociation of network states by other colorings, showing indirect effects. For example, focusing on circled "To Edges" simulations (Figure 5(a)), observe in Figure 6(d) how simulations with a minimum local overlapping level between possible paths have better performances than those with a higher local overlapping.

Note that simulations colored by overlapping criteria are split between two graphs (with local or global criteria) for clarity.

Identification of Indirect Effects of Assignment Parameters on TTD. To study in more detail the indirect effects, we split the simulations by demand pattern and plotted their final state colored by overlapping level, equilibrium criterion, or number of paths per OD. We observed the following correlations with TTD performance:

(a) Systematic positive correlation with a min local overlapping between paths:

For any pattern, simulations with this value of local overlapping are among the highest performers.

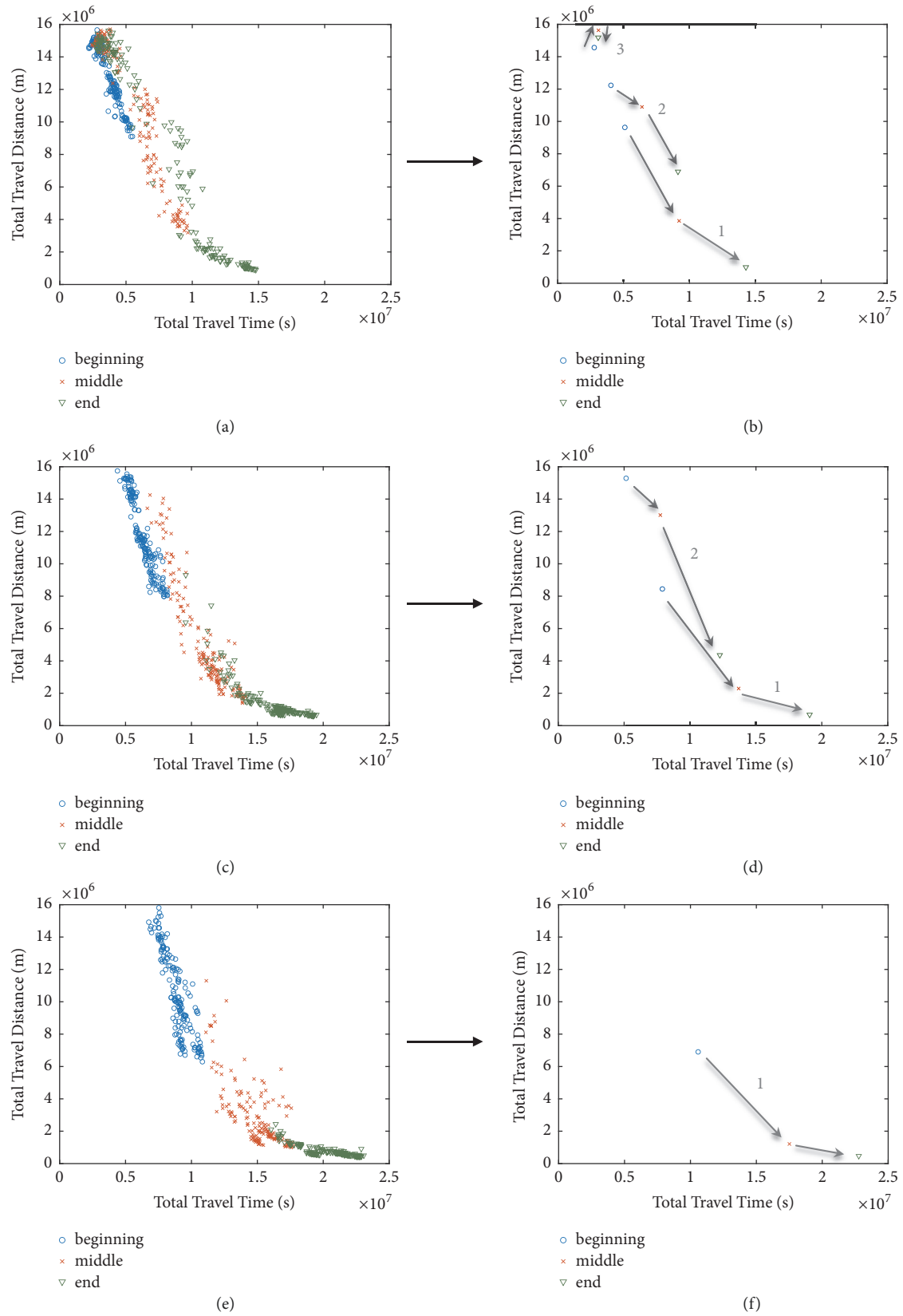
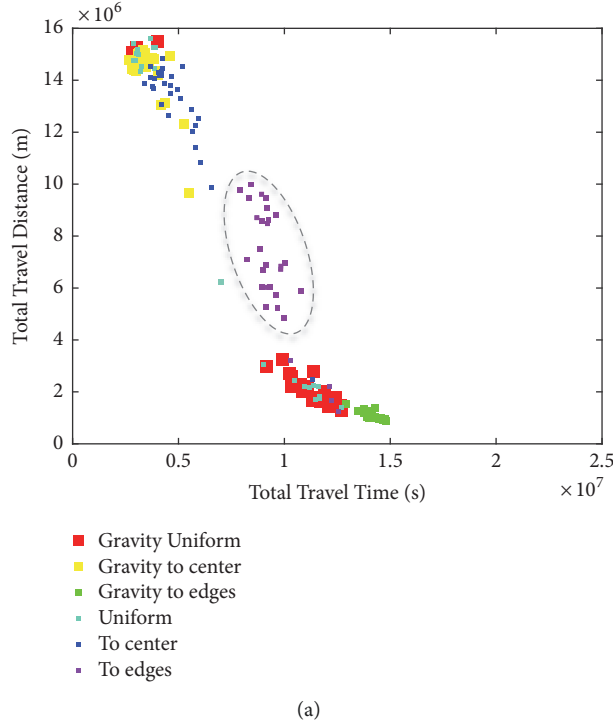


FIGURE 4: TTD performances: 1h30 simulations. Graphs (a), (c), and (e): evolution of all network states over time for demand levels 4, 5, and 6. Graphs (b), (d), and (f): some representative evolution cases for demand levels 4, 5, and 6.



<i>Demand pattern</i>	<i>Distance to travel (m)</i>	<i>TTD standard deviation</i>
'To center'	5.28×10^7	2.31×10^6
'To edges'	5.28×10^7	1.11×10^6
'Gravity to center'	5.28×10^7	2.40×10^6
'Uniform'	5.40×10^7	6.43×10^6
'Gravity Uniform'	5.49×10^7	4.66×10^6
'Gravity to edges'	5.67×10^7	0.15×10^6

(b)

FIGURE 5: (a) Final network states with demand level 4 colored by pattern and (b) table of metrics by pattern.

Depending on the pattern, these simulations keep a reasonable TTD score or even stay in a stable state. In Figure 7 an example of simulations with *convex but spread* pattern is plotted (Figure 7(a)) and an example with *bi-polar* pattern (Figure 7(b)).

(b) Sometimes positive correlation with UE criteria

With “To Edges,” “Uniform,” and “Gravity to Edges” patterns, simulations with a UE assignment criterion are clearly within the best performers. If we confirm the underlying effect of UE, it would mean that, in these cases, individual optimization (UE vs. BRUE) is beneficial for the system as well. Note that each of these patterns belongs to a different classification introduced above.

(c) Sometimes correlation with number of possible paths per OD

With “Gravity to Center” pattern, the simulations with the worst performances only have $p=3$ possible paths allowed per OD. With “Gravity Uniform” pattern, all the simulations with $p=3$ are among the worst performers and all the best performers have either $p=7$ or 9. With “Uniform” pattern, most of the simulations with $p=3$ are among the worst performers.

(d) Sometimes positive correlation with a relatively low global overlapping level

Although the best performances are usually related to a relatively low global overlapping, too few points are available to clarify the trend.

We shall note that the variability in the observed correlations and sometimes inversion effects may be explained by the following elements:

- Once separated by demand pattern, we only have few observation points that may furthermore not well explore the search space.
- There may be joined effects between the studied parameters, but we cannot observe them on these chosen graphs.
- There are sometimes some uncertainties in the parameters' design.

Deeper investigations will be provided later by the quantitative analysis of Sobol coefficients which permits us to statistically highlight first and higher order effects.

Gridlock Drop Rate. Now we are going to focus on the correlations between loading parameters and network states temporal heterogeneities to confirm the observed trends. As it was introduced in the Methodology section, we will study the *gridlock drop rate* metric to represent the TTD evolution over time.

The scattering of network states evolves over time. The *gridlock drop rate* (GDR) metric aims to capture this dynamic. As introduced in Figure 4, we calculated three values of TTD over the simulation time (blue and then orange and then green markers). For each simulation, we measure the TTD drop rate, relatively to the initial TTD score (i.e., after the 20-minute warm-up), by the middle and by the end of the simulation time. We keep the highest rate as the gridlock drop rate. Note that the GDR can be positive. This method allows

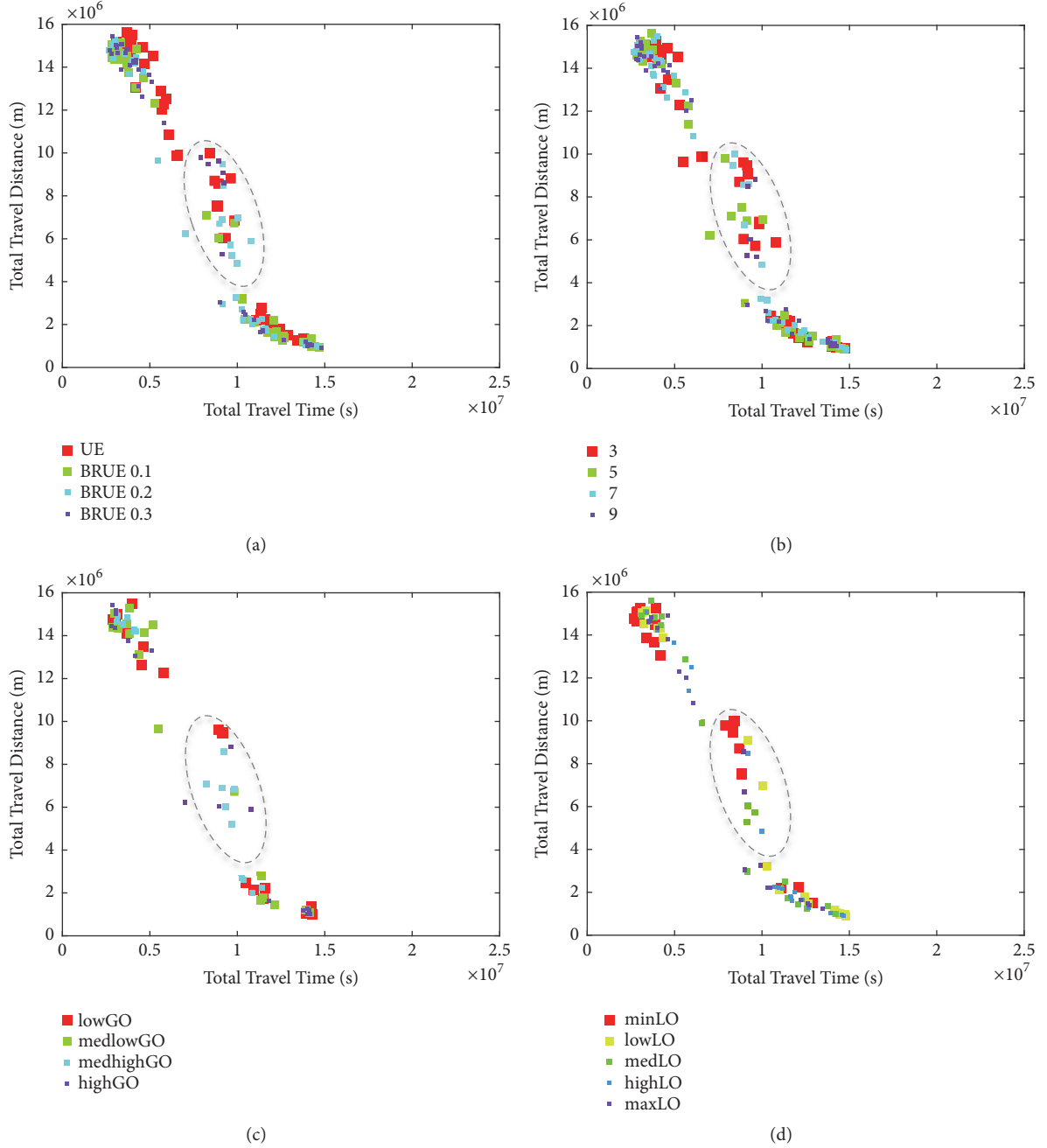


FIGURE 6: Final network states with demand level 4, colored by (a) equilibrium criterion, (b) number of paths per OD, (c) global overlapping level, or (d) local overlapping level.

us to capture the speed at which the network's initial TTD mostly changed to roughly reach its final state. Formally, the gridlock drop rate is calculated as follows:

$$GDR = \text{absmax} \left(\frac{TTD_{middle} - TTD_{initial}}{TTD_{initial} \times 20}; \frac{TTD_{end} - TTD_{initial}}{TTD_{initial} \times 40} \right) \quad (10)$$

where the function *absmax* returns the signed maximum absolute value, $TTD_{initial}$ is the initial TTD value, TTD_{middle}

is the TTD at the middle of the simulation, and TTD_{final} is the final TTD value. The percentage of drop is normalized by the time it took in minutes.

In Figure 8 the values of this GDR indicator against the TTT references for the simulations with demand levels 4, 5, or 6 are plotted. Simulations represented with a square experienced the highest drop of their $TTD_{initial}$ within the first 40 minutes of observation, whereas the triangle simulations experienced it in an hour.

Referring to Figure 8(a), we see that the distribution of gridlock drop rates is coherent with the network

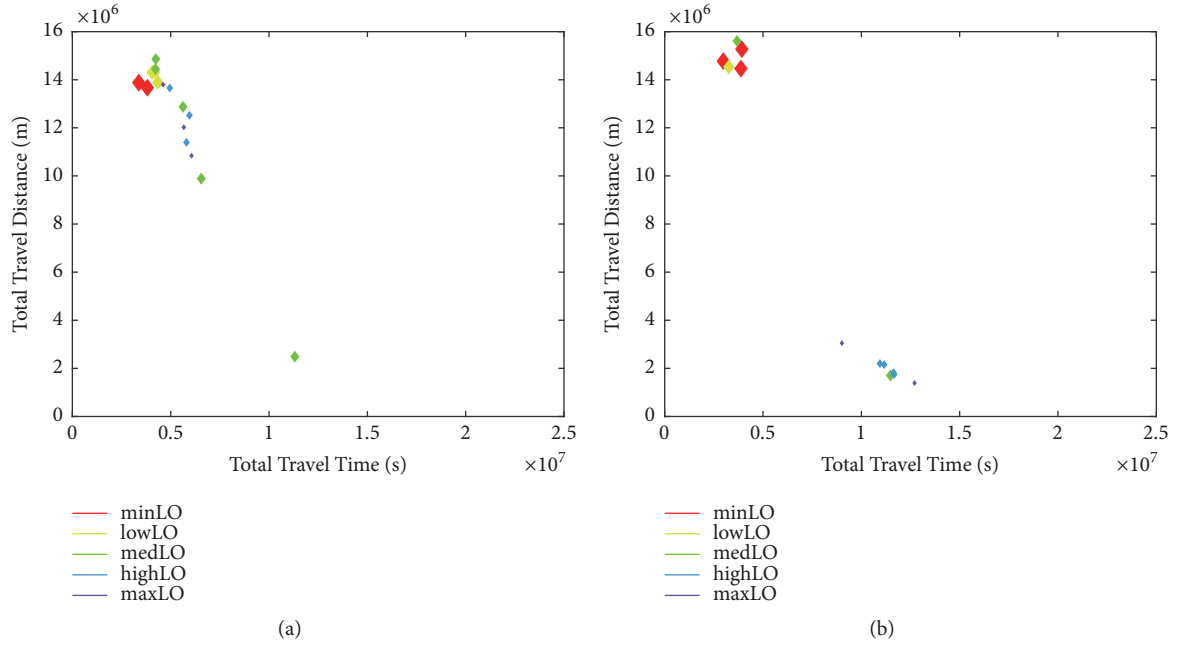


FIGURE 7: Final network states with demand level 4: examples of correlation with min local overlapping. (a) Case of “To Center” pattern and (b) case of “Uniform” pattern.

performances observed at the end of the 90-minute simulation time (ref. Figure 5(a)): the stable simulations’ highest change of $TTD_{initial}$ was around 0% per minute (that is to say none), while the other simulations’ highest change of $TTD_{initial}$ happened at a rate between -1%/min and -3.5%/min. For nonstable states with demand level 4, most of the gridlock drops happened in an hour. However, the steepest drops to gridlock already happened in 40 minutes. Most of the simulations in this latter case had a “Gravity to Edges” pattern. Figure 8(a) reveals again the classification of the simulations’ performance by the demand patterns in 3 types of clusters as seen in Figure 5(a). The same performance ranking by pattern is observed, revealing again the pattern direct effect.

When looking at further colorings, we also recognize the same performance correlations with the assignment parameters that we noted in the *indirect effects on TTD* paragraph.

In Figures 8(b) and 8(c) the simulations with the same loading parameters but a higher demand level are plotted: either 5 or 6. In both of these cases, simulations endure a high gridlock drop rate, with decreases of $TTD_{initial}$ above 2%/min. As opposed to demand level 4, most of the drops already happened in 40 minutes. For demand level 5, the only late drops had demand patterns “Gravity to Center” or “To Center.” For demand level 6, only few exceptions had a late drop.

Spatial Heterogeneity. We suspect that temporal heterogeneities, quantified by the *gridlock drop rate* (GDR) indicator, are closely related to final spatial heterogeneities (SH) among links’ average speed. Indeed, we can imagine that a transition to gridlock could be the result of one of these two

phenomena: either a local (possibly at multiple locations) and quick breakdown associated with high SH or a global and progressive breakdown associated with low SH. The value of SH was calculated at the end of each simulation for demand levels 4, 5, and 6. We found a 95% correlation between the final SH score and GDR for simulations with demand level 4, 85% correlation with demand level 5, and 60% correlation with demand level 6. These results confirm the above hypothesis of close relationship between SH and GDR.

Let us look closer at SH scores’ distribution on our simulation set with demand level 4, colored by variable value in Figure 9. Although GDR values were pretty linearly distributed, SH values present a clear breaking point delimiting a set of simulations with quite low (below 10) SH from a set of highly heterogeneous states.

An analysis of Figure 9 confirms that the level of demand, demand pattern, and minimum local overlapping are really the dominant factors on the possible network performances. Furthermore, a UE criterion or the number of possible paths per OD seems to influence traffic conditions by combined effects. The same correlations as the ones noted with TTD are observed and confirm the relation assumed between SH and TTD: a low TTD score is correlated with a high SH score and vice versa.

3.1.2. Analysis of Simulations with Dynamic Assignment. More frequent assignment periods allow the adjustment of the path flow distribution to the dynamic evolution of traffic conditions. We called this “dynamic assignment” in Section 2.1.2(2), as opposed to the “static assignment” we performed and analyzed in Section 3.1.1., where we had a single assignment period for the whole 90-minute simulation.

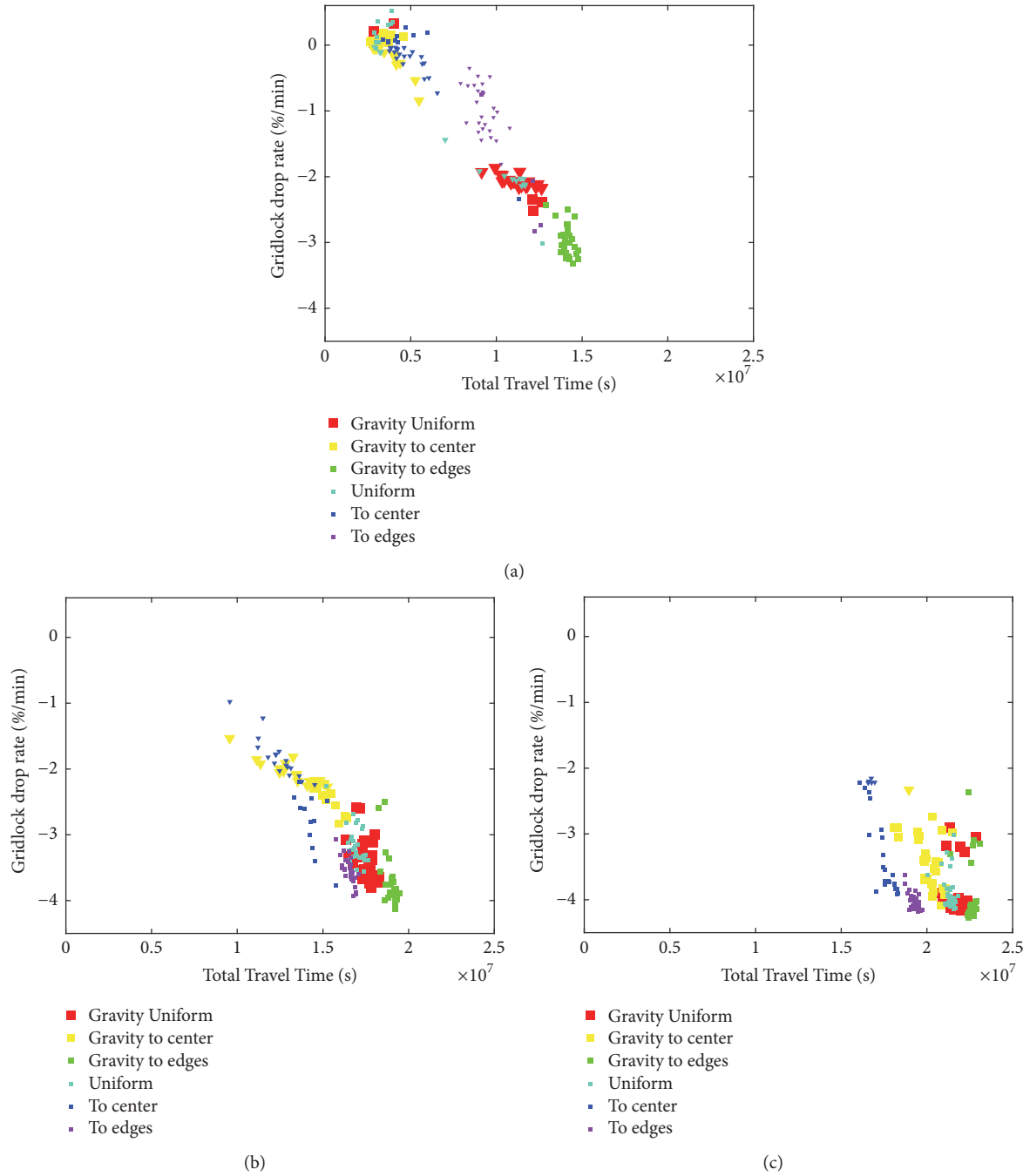


FIGURE 8: Gridlock drop rate colored by pattern. (a) Demand level 4, (b) demand level 5, and (c) demand level 6.

This method corresponded to an average choice with average travel times, simulating a day-to-day traffic assignment routine.

Just as in Figure 4, Figure 10 displays the evolution of the simulations' TTD score over time for the same 3 higher levels of demand (4, 5, and 6), but this time with a traffic assignment revised every 20 minutes. A dash line was plotted to remember the TTD higher boundary reached with static assignment in Figure 4. While the TTD scale was extended, the TTT scale was maintained.

We shall first note that dynamic assignment improves the average network performances. While some networks now keep stable traffic conditions with demand levels 4 or 5 (examples of maintained TTD score in Figures 10(a) and 10(b)), others still did not reach such gridlocked final states as they did with static assignment. However, with demand level 6, most of the final network states have a TTD below 2×10^6 m, wherever the assignment was dynamic (Figure 4(e)) or static (Figure 10(c)). This shows that, even with dynamic assignment, the demand level remains the

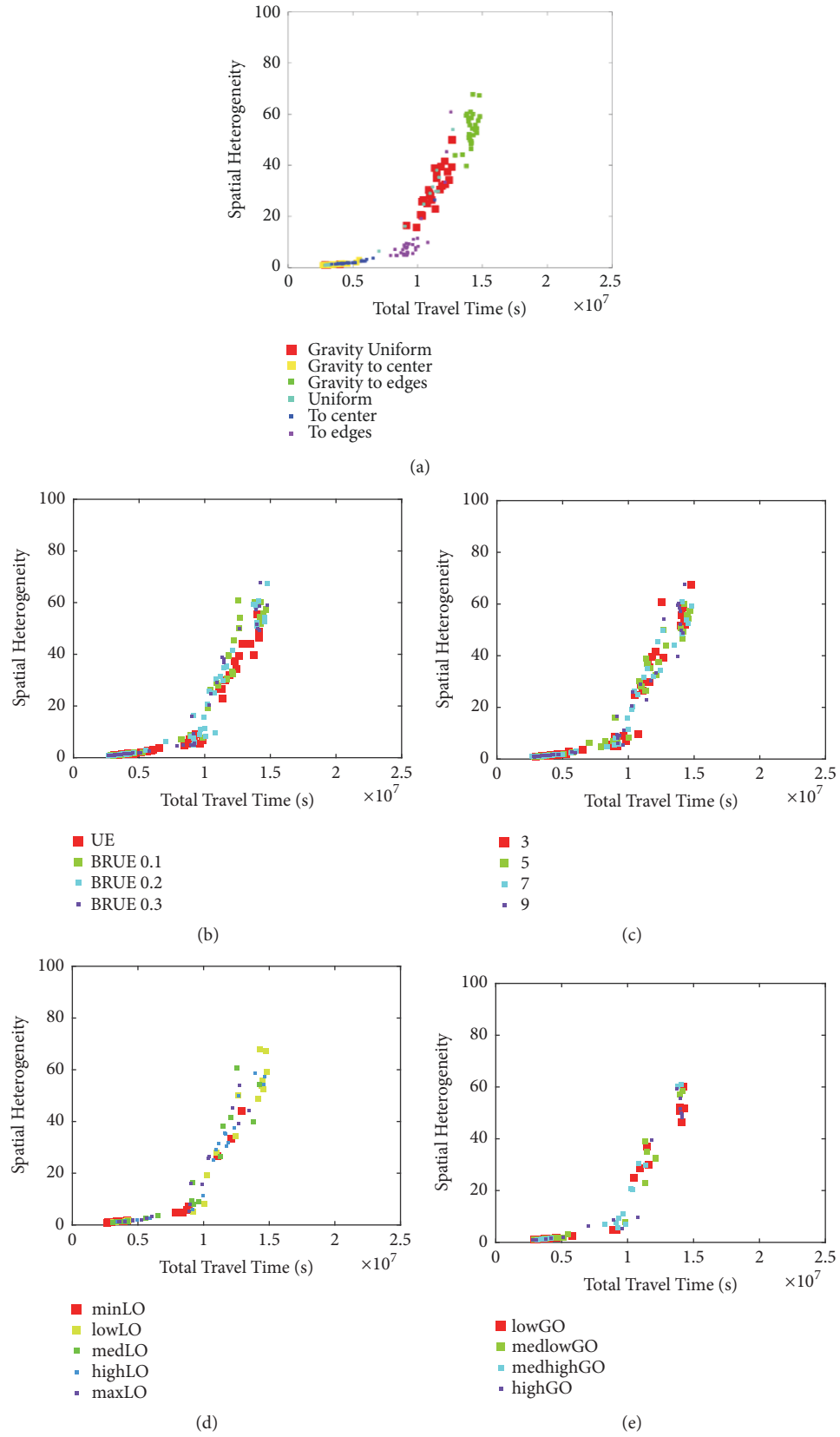


FIGURE 9: Spatial heterogeneity of simulations' final state with demand level 4, colored by (a) demand pattern, (b) equilibrium criterion, (c) number of paths per OD, (d) global overlapping level, or (e) local overlapping level.

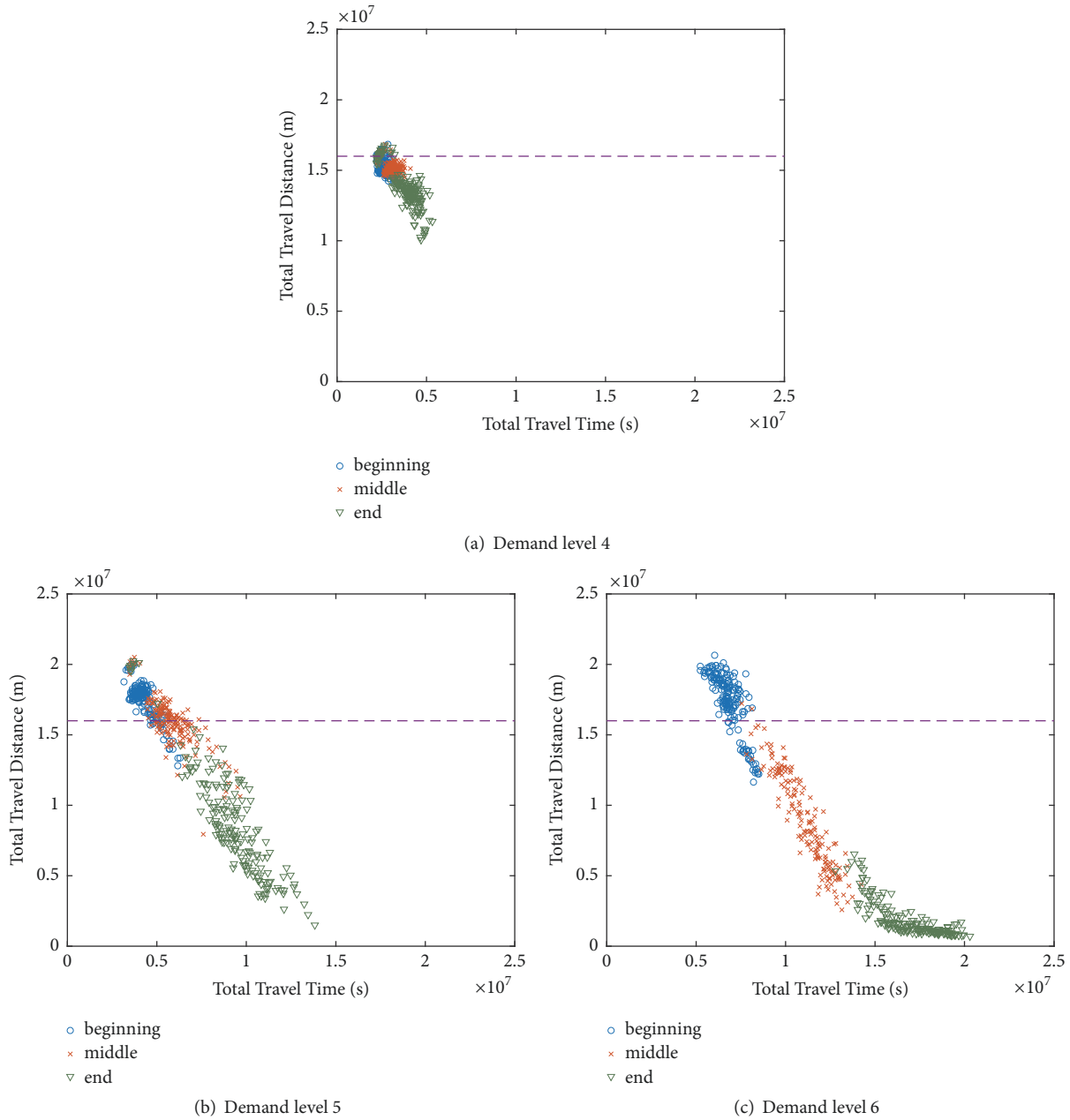


FIGURE 10: TTD performances: 1h30 simulations with dynamic assignment. (a) Demand level 4, (b) demand level 5, and (c) demand level 6.

main factor influencing traffic conditions. However, how did the effect of the loading parameters on network performances change with dynamic assignment?

Figure 11 displays the simulations' gridlock drop rate. Note that a zoom on the network states was made in Figure 11(a) for readability; thus the scale is different from all the other graphs presenting gridlock drop rates.

Comparing Figure 8 to Figure 11, we note that, while there is a clear effect of dynamic assignment on slowing or inhibiting the gridlock drop rate for demand levels 4 and 5 (scores distributed in tighter intervals closer to 0), the distribution of this performance score remains very similar with demand level 6. Furthermore, looking at the triangle

vs. square markers in Figure 8 vs. Figure 11, observe how, with dynamic assignment, the simulations' highest change of $TTD_{initial}$ now happens later, at least after 40 minutes of simulation. With demand levels 4 or 5, there is almost no earlier drop, while with demand level 6, this proportion is now reduced to two thirds.

To better understand these various journeys to gridlock phenomena, let us study the final spatial heterogeneities and their link to the gridlock drop rate. In Figure 12 the spatial heterogeneities of networks' final states corresponding to the simulations with dynamic assignment are plotted. Compared to the case of static assignment, note that the distributions of this score now live in smaller intervals

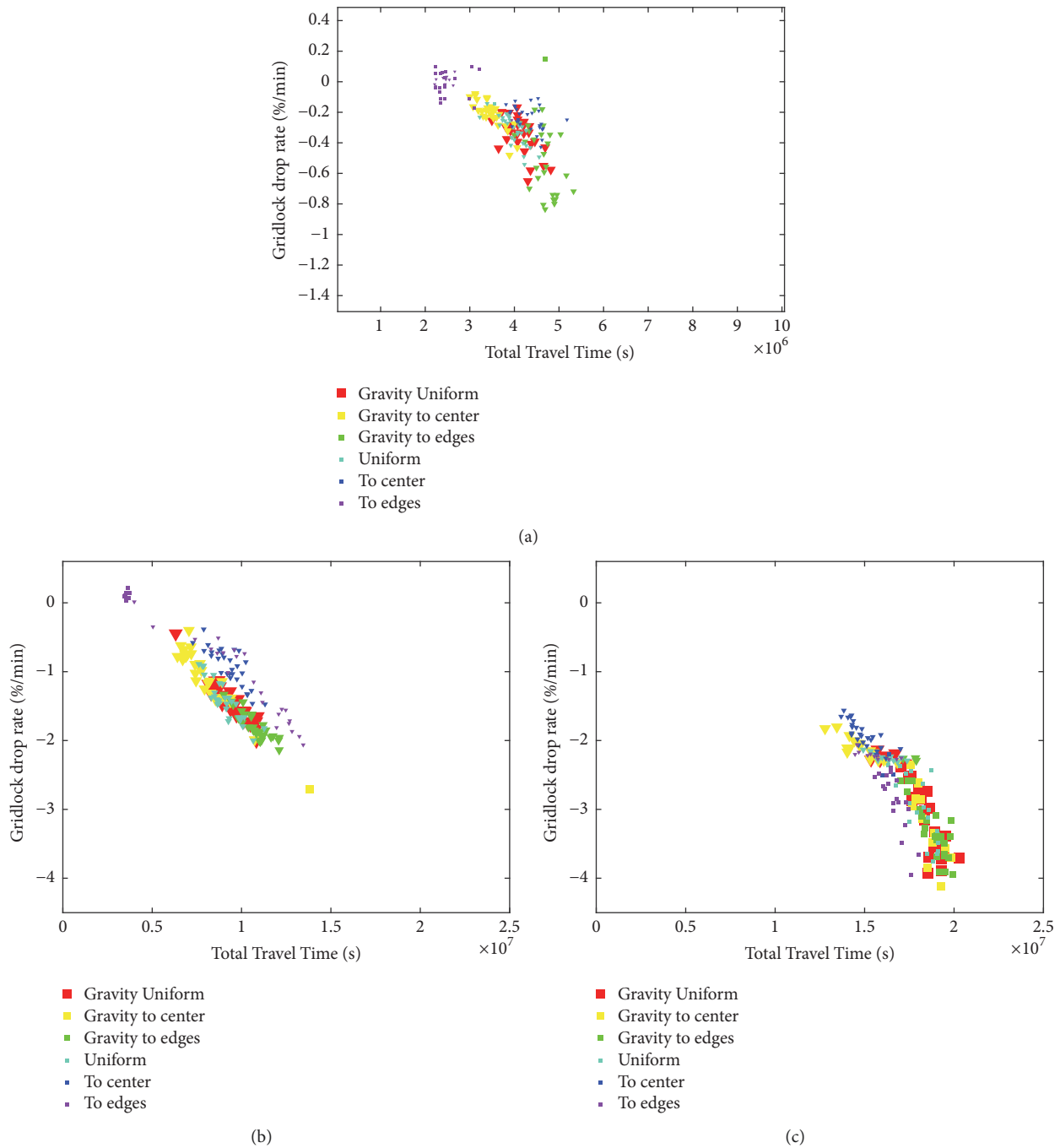


FIGURE 11: Gridlock drop rate: 1h30 simulations with dynamic assignment. (a) Demand level 4, (b) demand level 5, and (c) demand level 6.

closer to 0, especially for demand levels 4 and 5, like GDR.

We found a 86% correlation between the final SH score and GDR for simulations with demand level 4, 80% correlation with demand level 5, and 90% correlation with demand level 6. This shows a close relationship between SH and GDR also in the case of dynamic assignment.

Reassignment permits a more reactive and resilient system: it leads to lower heterogeneities and stabilizes situations that would have converged to gridlock when the demand level

stays reasonable. But which role did the loading parameters play in the case of dynamic assignment?

The gridlock drop rates and spatial heterogeneities were colored by demand pattern parameter in Figures 11 and 12. We immediately identify that this variable induces a much less clear clustering of simulations' performances than with static assignment, calling for lower effect of this parameter. Moreover, it looks like the relative performance between simulations changed. To observe the effects of the assignment parameters in more detail, we will focus on final TTD states

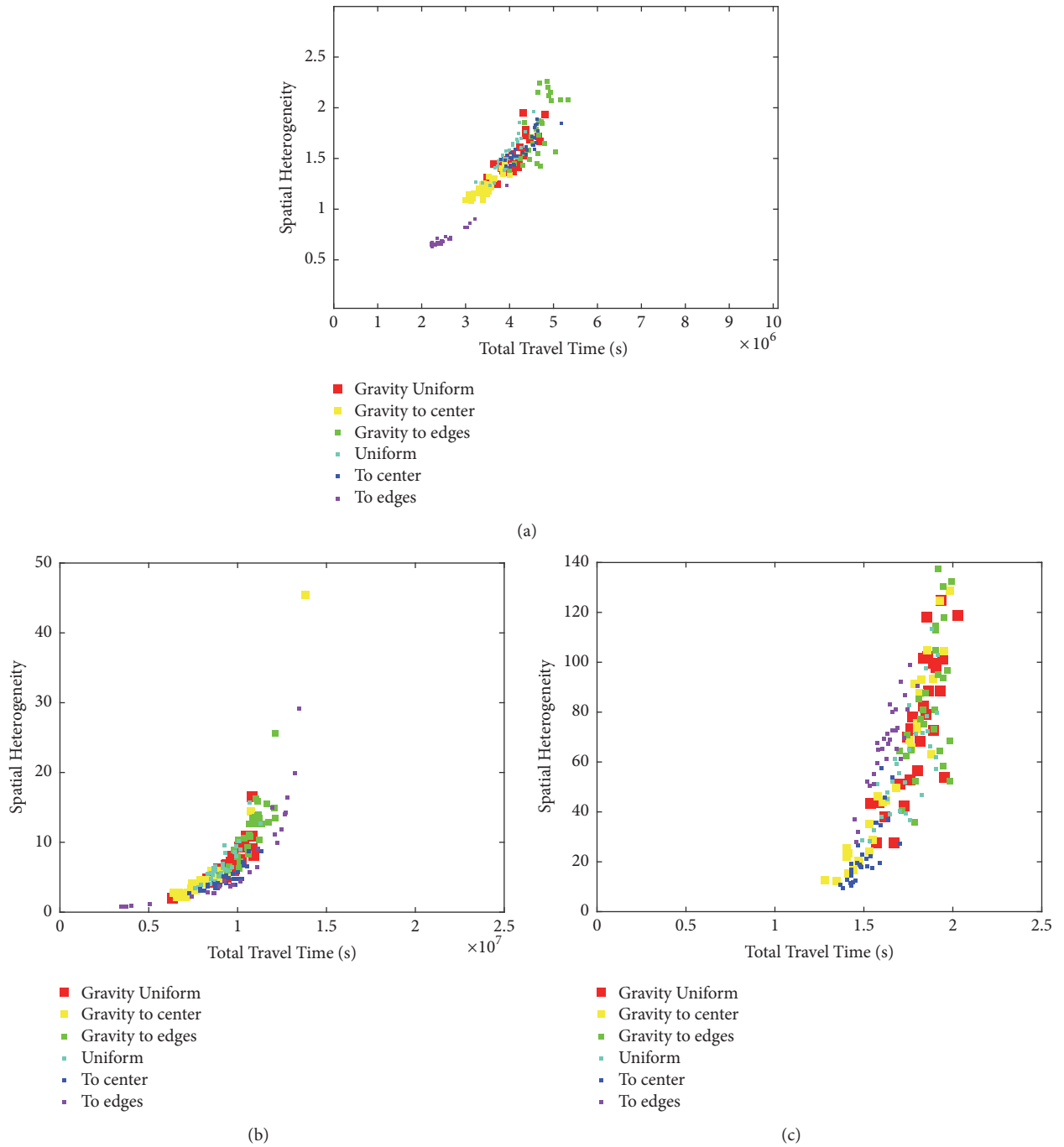


FIGURE 12: Spatial heterogeneity of simulations' final state: 1h30 simulations with dynamic assignment. (a) Demand level 4, (b) demand level 5, and (c) demand level 6.

with demand level 5, since this simulation set experiences the most influence of the studied variables. The TTD performances plotted in Figure 13 are colored by assignment parameter.

Although the equilibrium criterion and global overlapping score parameters do not seem to have direct effects, it looks like the number of paths per OD and local overlapping score parameters now show a direct effect: the min local overlapping level is associated with better TTD performances

(Figure 13(d)), while simulations with a high number of paths per OD are, as opposed to the ones with only $p=3$ paths allowed, associated with better performances (Figure 13(b)). These direct correlations can clearly be seen on the temporal and spatial heterogeneities in Figures 14 and 15 as well.

Nevertheless, each of these direct effects appears to be weaker than the one of demand pattern parameter on simulations with static assignment, calling for a higher proportion of indirect effects in the case of dynamic assignment. In fact,

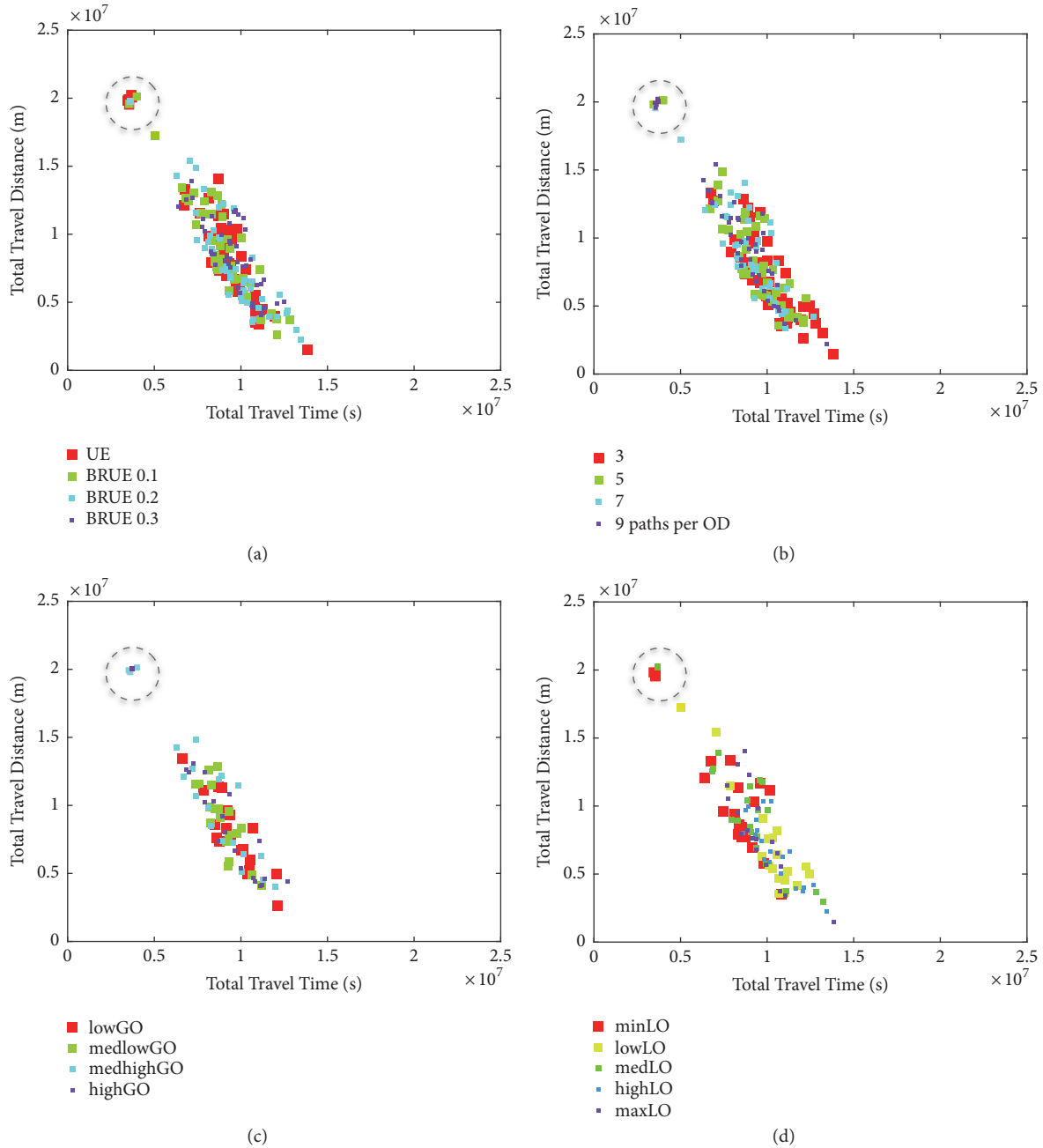


FIGURE 13: Final network states with demand level 5 and dynamic assignment, colored by (a) equilibrium criterion, (b) number of paths per OD, (c) global overlapping level, or (d) local overlapping level.

we can observe the example of the stable states, circled by a dash line in Figure 13. All these simulations underwent the same demand pattern “To Edges,” which extrapolates a wide variety of network states. But what actually keeps these cases in stable state is a combination of parameters that have shown to be associated with best performances: a high number of possible paths, rather strict equilibrium criteria, and minimum local overlapping.

3.2. Quantitative Analysis. In this part, we conduct a variance-based sensitivity analysis of the performance

indicators produced by our simulations. We present results from Sobol indices calculation and complete conclusions highlighted in our graphical analysis.

The chosen quantitative sensitivity analysis method aims to explain the variance of an output by the variance of inputs. We shall note that the produced Sobol indices are relative to the performance indicator’s variance, calculating the proportions in which our network loading parameters are responsible for this variability. Thus, it is important to first recall the disparities among the variances of the performance indicators.

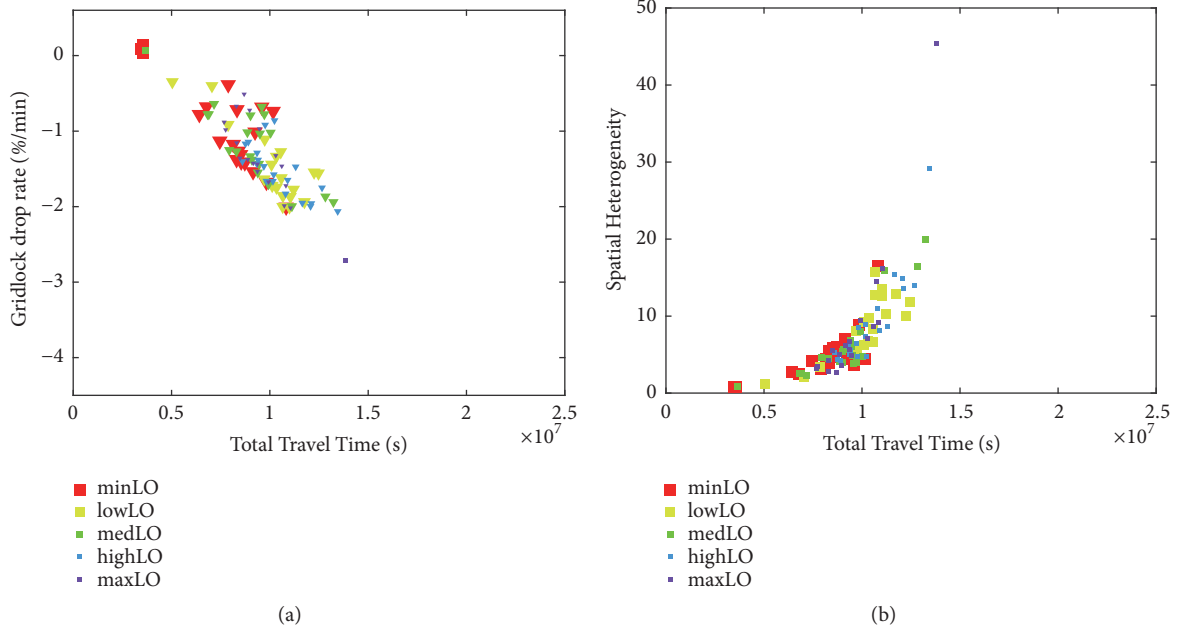


FIGURE 14: Network heterogeneities with demand level 5 and dynamic assignment, colored by local overlapping level. (a) Gridlock drop rate and (b) spatial heterogeneity.

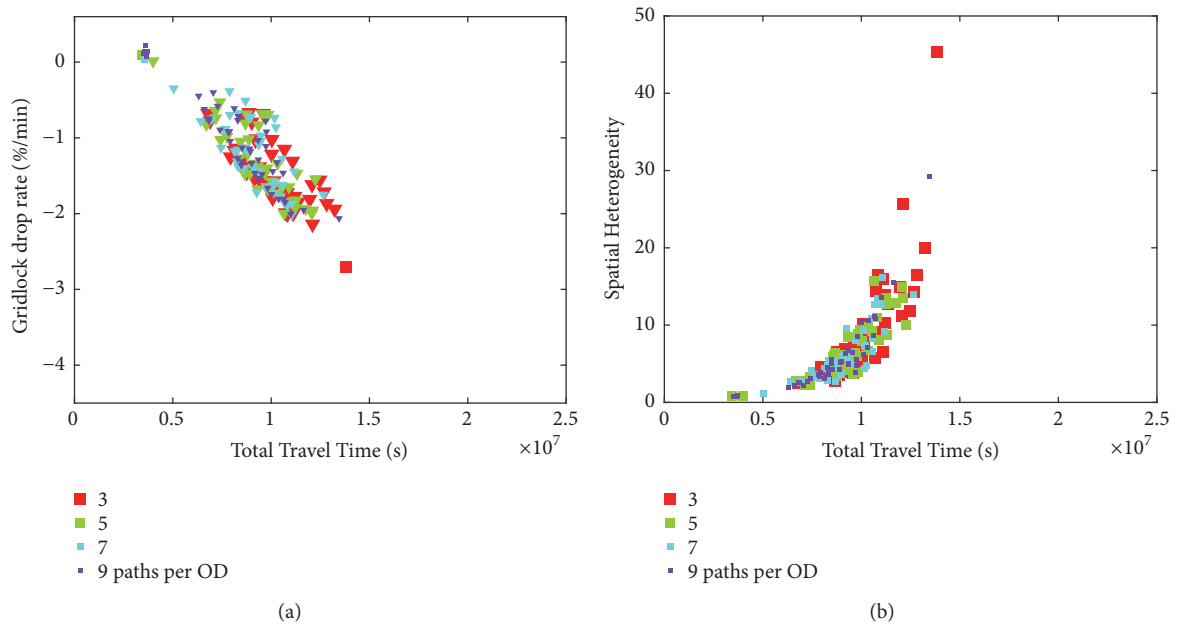


FIGURE 15: Network heterogeneities with demand level 5 and dynamic assignment, colored by number of paths per OD. (a) Gridlock drop rate and (b) spatial heterogeneity.

For each of the 6 case studies, Table 1 presents the variance of the simulations' network performance scores. Note that, since TTD, TTT, and Mean Network Speed indicators are closely related, only TTD was kept as a reference.

To support our quantitative analysis, we represented in Figure 16 the significant Sobol indices of only 3 over 6 case studies, underlined in Table 1, chosen because of two reasons:

(i) Their significant performances' variance

(ii) From one case to another, only the demand level or the assignment frequency (static vs. dynamic) changes; this will allow us to distinguish the effect of these two variables

The standard error of the Sobol indices oscillates between 0.001 and 0.02.

In Figure 16, the pie chart shows the proportion in which each order of effect explains the variance of the given

TABLE 1: Distribution indicators for the main network performance scores.

Variance	Final TTD (10^{12} m)	Gridlock Drop Rate (%/min)	Final Spatial Heterogeneity
<i>Static & Demand level 4</i>	<u>34.224</u>	<u>1.4302</u>	<u>441.75</u>
<i>Static & Demand level 5</i>	<u>1.6695</u>	<u>0.5070</u>	<u>1066.70</u>
<i>Static & Demand level 6</i>	0.1251	0.2797	1342.60
<i>Dynamic & Demand level 4</i>	1.9648	0.0381	0.15
<i>Dynamic & Demand level 5</i>	<u>15.236</u>	<u>0.2824</u>	<u>29.08</u>
<i>Dynamic & Demand level 6</i>	1.6493	0.4076	964.42

performance indicator. Each column of the bar chart presents the Total Sobol indices (i.e., the total effect) of the given network loading parameter, as the sum of its first order effect (in yellow), the involved 3 second order effects (in orange), and the 3 third order effects together with the forth order effect (in grey). Second order effects shared between columns contain the same markers for easy visual pairing.

From Figure 16(a) to Figure 16(b), A Rise in Demand Level. Concerning TTD performances, the total effects of the pattern and equilibrium criteria lower for the benefit of the overlapping and number of paths total effects. While the decreases are due to the drop of the pattern 1st order effect (75% down to 50%) and its pairwise interaction with the equilibrium criterion (6% down to 0%), the 50% increases in total effects for the overlapping and number of paths are due to a raise of their 1st order effect, their 2nd order effect with the pattern, and their pairwise effect. These results indicate that the rise of demand level doubled the influence of the overlapping level and number of paths on the simulations final TTD states.

The trends observed in Figure 16(a) confirm what we observed in the graphical analysis, within the paragraphs “Identification of direct effects of loading variables on TTD” and “Identification of indirect effects of assignment parameters on TTD” in Section 3.1.1.

Looking at the graph presenting the final states in terms of TTD and TTT for demand level 5, we note that the rise of demand level led to a high proportion of final network states at gridlock. Most of the simulations then explaining the TTD variance have one of two pattern values without distinction on performances. The other scores are clustered for the other pattern values. On the other hand, the spread simulations have a performance well distinguished by their overlapping and number of paths values. This may explain the variation in measured effects.

Concerning GDR performances, although the variance is in both cases 80% due to 1st order pattern effect, the 8% due to 2nd order effects, coming from the pattern interaction with the overlapping or the equilibrium criterion, disappear to the benefit of 3rd or 4th order effects. With static assignment, the pattern value alone can explain most of the GDR performance. Although with demand level 4 half of the remaining influence was still due to a combination of two parameters only, with demand level 5 any additional influence requires the combination of at least 3 network loading values.

Concerning SH performances, while the proportion of 3rd and 4th order effects stays still, the proportion of variance that was explained by the 2nd order pattern-overlapping effect is now mostly due to a higher 1st order effect of the pattern. Thus, while the total effect of the pattern, number of paths, or eq. criteria stays still, the total effect of the overlapping decreases by two thirds.

From Figure 16(b) to Figure 16(c), from Static to Dynamic Assignment. Concerning TTD performances, although the variance is in both cases 70% due to 1st order effects, there is a proportion inversion between 2nd and 3rd order effects. For the 2nd order effects, while the pattern-overlapping and overlapping-nbP effects disappear, the interaction pattern overlapping is divided by two. These drops are compensated by a rise of 3rd and 4th effects. As for 1st order effects, we observe a 12% decrease of the overlapping to the benefit of an increase for the pattern and number of paths.

Concerning GDR performances, 1st order effects proportion goes down to explaining 60% of GDR variance: the pattern contribution goes from 80% to 40% while the other 20% are spread between overlapping (for half), number of paths, and equilibrium criterion (a forth each). A 2nd order pattern-overlapping effect now accounts for 10% of GDR variance. The last 30% of GDR variance is explained mostly by interactions between the pattern, number of paths, and equilibrium criterion.

The overlapping influence increases mostly because of 1st order and 2nd order effect with the pattern while number of paths and eq. criterion ‘s influences increase mostly because of 3rd and 4th order effects with the pattern.

Concerning SH performances, 1st order effects go from explaining 90% of SH’s variance to explaining only 40%: the influence of the pattern went from 80% to now only 30% 1st order, while its 2nd order effects with the overlapping and with the equilibrium criterion now account for 10% each. The last 44% of SH’s variance are explained by 3rd and 4th order effects.

Overviewing all the performance indicators for these three case studies, the demand pattern parameter is always the major contributor in the 1st order effects and 2nd order effects. The most significant 2nd order effect emerges from its association with the overlapping parameter and then with the equilibrium criterion and then with the number of paths. The 4th most significant 2nd order effect comes from the joined action of the overlapping and number of paths settings. The

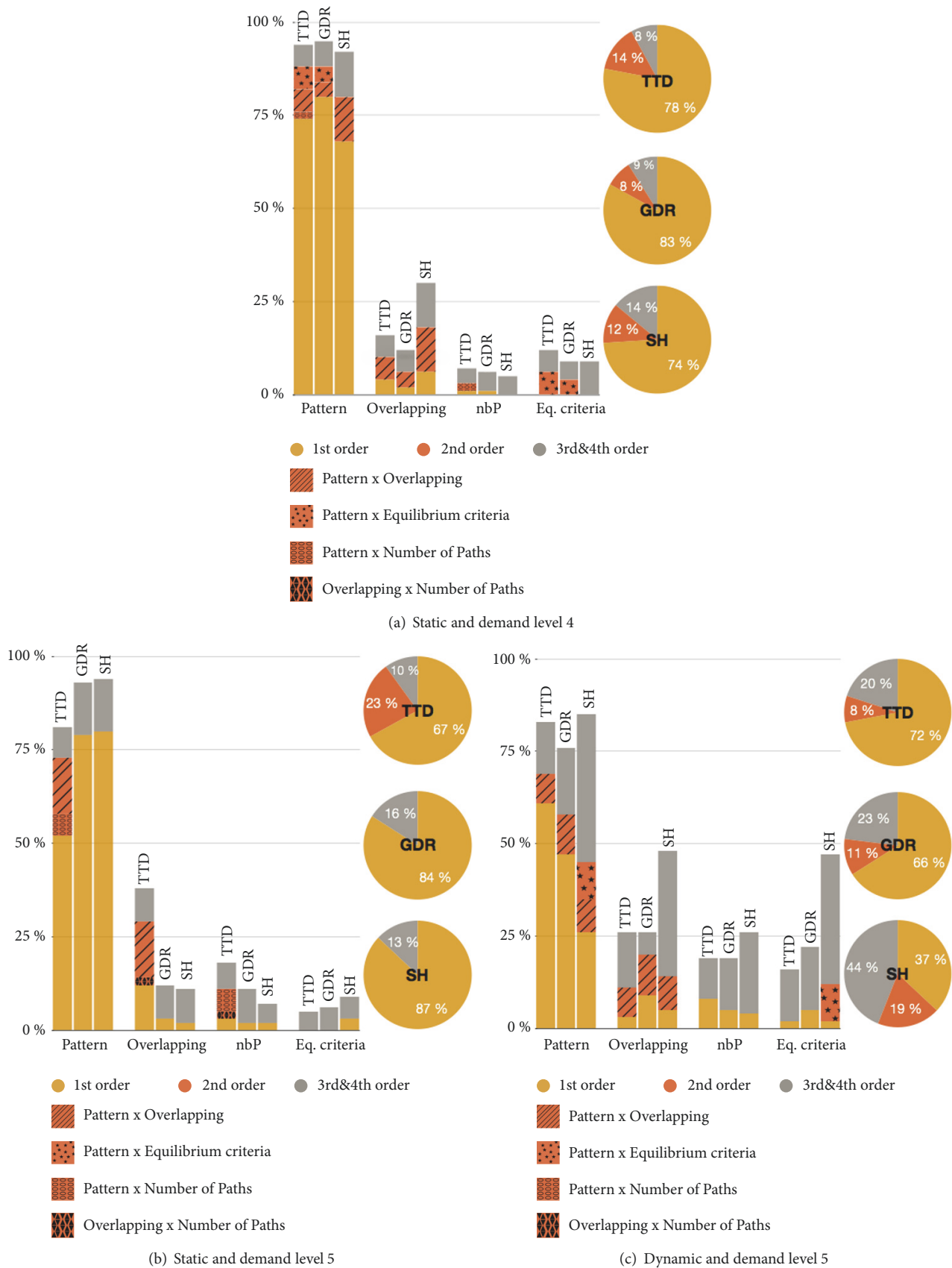


FIGURE 16: Presentation of Sobol indices for three representative case studies.

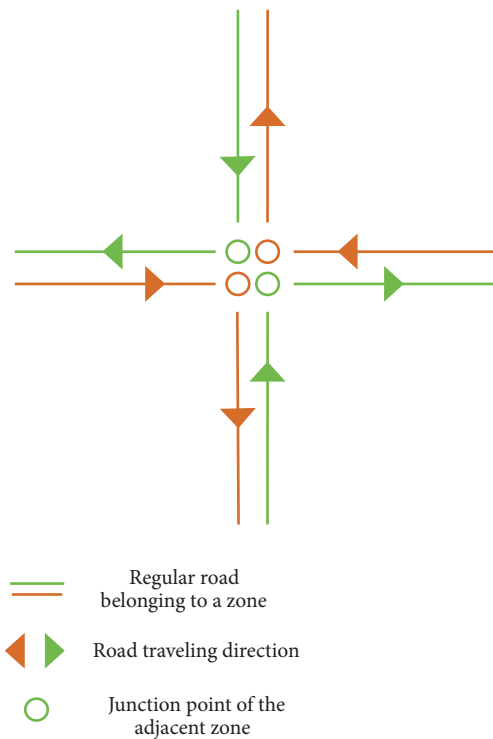


FIGURE 17: Details of an intersection of regular roads between 4 zones.

pattern is so dominant that it will not really let the other loading parameters live by themselves.

With static assignment (Figures 16(a) and 16(b)), the pie charts show that more than 70% of the effects of network loading parameters on performance levels are due to 1st order effects. At least 50% of these 1st order effects are due to the pattern parameter.

Compared to the static cases, with dynamic assignment (Figure 16(c)) the global influence of the pattern parameter is only slightly lower, but its effect becomes more indirect: higher order effects increased from 1/4 to about 1/2 of the total effects. This increase comes with an escalation of the total indices of the overlapping, number of paths, and equilibrium criteria, mostly related to an augmentation of indirect effects. Indeed, a dynamic assignment process refreshes path flow distribution more often and thus allows us to better optimize the network capacities which are highly dependent on the overlapping level, number of possible paths, and equilibrium criterion. These observations strengthen the visual analysis of Figures 11, 12, and 13.

A tentative calculation of Sobol indices with fixed demand pattern was performed for two demand patterns showing variability in their final states for the 3 case studies chosen in our Sobol analysis: “To Center” and “To Edges” patterns. Due to the lower number of observation points, the accuracy of the Sobol indices is a little lower, with a standard error ranging between 0.06 and 0.1. Only the TTD performance parameter is analyzed below, since noticeable trends are very similar for the GRD and SH indicators.

With “To Center” Pattern. In the case study with demand level 4 and static assignment, there are no relevant 1st or 2nd order effects. The total contribution of each of the 3 variables (only due to the 3rd order indices) is thus the same and is close to 1.

In the case study with demand level 5 and static assignment, the number of paths accounts by itself for 18% of the TTD variance, while the overlapping explains 14%. The interaction of these two parameters accounts for 60% of the performance’s variance.

In the case study with demand level 5 and dynamic assignment, the overlapping explains by itself 55% of the TTD variance and interacts with the number of paths to explain 20% more.

Even if the 3 remaining parameters had the same proportion of influence in the case with demand level 4 and static assignment, with a higher demand level but still a static assignment, the number of paths and overlapping parameters took the lead, especially by interaction effect. In the case with demand level 5 and dynamic assignment, the overlapping parameter imposes itself as the main influencer.

With “To Edges” Pattern. In the case study with demand level 4 and static assignment, 60% of the TTD variance is explained by the equilibrium parameter by itself while another 26% is explained by its interaction with the overlapping criterion.

In the case study with demand level 5 and static assignment, 30% of the TTD variance is explained by the overlapping criteria by itself. Most of the performance variance is explained by 2nd order effects: 58% of overlapping-number of paths interaction, 10% of number of paths-equilibrium criterion interaction, and 15% of overlapping-equilibrium criterion interaction.

In the case study with demand level 5 and dynamic assignment, most of the TTD variance is explained by 1st order indices: 30% contribution of the overlapping, 20% contribution of the number of paths, and 15% contribution of the equilibrium criterion. An additional 30% are explained by the number of paths-overlapping second order effect.

Even if the equilibrium criterion stood up as the main influencer in the case with demand level 4 and static assignment, a rise of demand came with a higher impact of the overlapping and its interaction with the number of paths. A dynamic assignment came with a more balanced distribution of effects but mostly explained by the values of the overlapping and number of paths.

For a given case study, depending on the demand pattern, the effects of the number of paths, overlapping, and equilibrium varies. Although we can draw systemic conclusions, attention should be given to the case study.

4. Conclusions

In this paper, we conducted a Global Sensitivity Analysis of network performances to all network loading parameters. These parameters aimed to represent a wide range of the possible OD matrix, path selected sets, and flow distributions, so as to explore all situations of demand that an urban network could realistically undergo. The implemented

More precisely, for a given demand level and demand pattern setting, we observed that paths sets with no overlapping at the OD level were systematically correlated with the highest network performances, in some settings a UE assignment criterion or a high number of alternative paths was clearly associated with best performances while in others a restricted number of alternative paths was correlated with the worst network performances. Our analysis did not show a progressive impact among the variety of values taken by each loading parameter but rather the positive or negative impact of some specific values only.

This study also revealed a strong relation between the gridlock drop rate (GDR) and the spatial heterogeneity (SH) among network states, explained as follows. A transition to gridlock could be the result of one of these two phenomena: either a local (possibly at multiple locations) and quick breakdown associated with high SH, or a global and progressive breakdown associated with low SH. From an operational point of view, slower transitions to gridlock offer more possibilities to handle traffic, favorable for a resilient city.

Finally, we studied the impact of a dynamic assignment process where the equilibrium is updated every 20 minutes instead of calculating for the whole simulation time. As expected, dynamic assignment improves the average network performances; it stabilizes some networks state and it delays and smoothers the speed to gridlock. The relation between the GRD and the SH stays as strong. Dynamic assignment limits the direct effect of the demand pattern parameter while increasing the direct overlapping and number of paths parameters. The effects of the network loading parameters on the observed performances rather result from their specific combinations.

This paper brings insights on how much the performances of a network can depend on loading parameters. The methods implemented in this study could easily be used for additional Global Sensitivity Analysis. Further work may be conducted on more specific networks to account for the diversity of topology. It may also be interesting to study more flexible OD matrix in the space and time dimensions.

Data Availability

This study is not based on real data. However, for reproducibility, the complete description of the simulation input settings is described in Section 2 of the paper. The simulations were performed by the Symuvia software tool, developed internally in the LICIT laboratory. The process of open sourcing the tool is in progress.

Conflicts of Interest

The authors declare that there are no conflicts of interest regarding the publication of this article.

Acknowledgments

This project is supported by the European Research Council (ERC) under the European Union's Horizon 2020 Research

and Innovation Program (grant agreement No. 646592 - MAGnUM project).

References

- [1] A. Abdulhafedh, "Advances in Dynamic Traffic Assignment Models," *International Journal of Traffic and Transportation Engineering*, vol. 6, no. 1, pp. 1–7, 2017.
- [2] W. Y. Szeto and H. K. Lo, "Dynamic traffic assignment: review and future," *Journal of Transportation Systems Engineering and Information Technology*, vol. 5, no. 5, pp. 85–100, 2005.
- [3] S. Peeta and A. K. Ziliaskopoulos, "Foundations of dynamic traffic assignment: the past, the present and the future," *Networks and Spatial Economics*, vol. 1, no. 3–4, pp. 233–265, 2001.
- [4] T. De la Barra, T. B. Perez, and J. Anez, "Multidimensional Path Search and Assignment," in *In Proceedings of the 21st PTRC Summer Meeting*, pp. 307–319, 1993.
- [5] M. Ben-Akiva, M. J. Bergman, A. J. Daly, and R. Ramaswamy, "Modelling ter Urban Route Choice Behaviour," in *Proceedings of the 9th International Symposium on Transportation and Traffic Theory*, J. Volmuller and R. Hamerslag, Eds., pp. 299–330, VNU Press, Utrecht, 1984.
- [6] B. Ciuffo, V. Punzo, and E. Qualietta, "Kriging meta-modelling to verify traffic micro-simulation calibration methods," in *Proceedings of the 90th Transportation Research Board Annual Meeting*, Washington DC., USA, 2011.
- [7] V. Punzo and B. Ciuffo, "How parameters of microscopic traffic flow models relate to traffic dynamics in simulation: Implications for model calibration," *Transportation Research Record*, no. 2124, pp. 249–256, 2009.
- [8] V. Punzo and B. Ciuffo, *Sensitivity Analysis of Car-Following Models: Methodology and Application*, Presented at 90th Annual Meeting of the Transportation Research Board, USA, Washington DC, 2011.
- [9] B. Ciuffo, V. Punzo, and M. Montanino, "Global sensitivity analysis techniques to simplify the calibration of traffic simulation models. Methodology and application to the IDM car-following model," *IET Intelligent Transport Systems*, vol. 8, no. 5, pp. 479–489, 2014.
- [10] V. Punzo, M. Montanino, and B. Ciuffo, "Do we really need to calibrate all the parameters? Variance-based sensitivity analysis to simplify microscopic traffic flow models," *IEEE Transactions on Intelligent Transportation Systems*, vol. 16, no. 1, pp. 184–193, 2015.
- [11] Q. Ge and M. Menendez, "An improved approach for the sensitivity analysis of computationally expensive microscopic traffic models: a case study of the Zurich network in VISSIM," in *Proceedings of the 92th transportation research board annual meeting*, Washington DC, USA, 2013.
- [12] Q. Ge, B. Ciuffo, and M. Menendez, "Comprehensive approach for the sensitivity analysis of high-dimensional and computationally expensive traffic simulation models," *Transportation Research Record*, vol. 2422, pp. 121–130, 2014.
- [13] Q. Ge, B. Ciuffo, and M. Menendez, "An exploratory study of two efficient approaches for the sensitivity analysis of computationally expensive traffic simulation models," *IEEE Transactions on Intelligent Transportation Systems*, vol. 15, no. 3, pp. 1288–1297, 2014.
- [14] Q. Ge, B. Ciuffo, and M. Menendez, "Combining screening and metamodel-based methods: An efficient sequential approach for the sensitivity analysis of model outputs," *Reliability Engineering & System Safety*, vol. 134, pp. 334–344, 2015.

- [15] Q. Ge and M. Menendez, "An Efficient Sensitivity Analysis Approach for Computationally Expensive Microscopic Traffic Simulation Models," *International Journal of Transportation*, vol. 2, no. 2, pp. 49–64, 2014.
- [16] T. Djukic, "Marginal effects evaluation with respect to changes in OD demand for dynamic OD demand estimation," in *Proceedings of the International Conference on Intelligent Transport Systems in Theory and Practice, mobil. TUM '17*, Munich, Germany, 2017.
- [17] R. Chen, V. Mallet, V. Aguilera et al., "Global Sensitivity Analysis in the Simulation of Road Traffic Emissions at Metropolitan Scale," *Proceedings TAP*, 2017.
- [18] R. L. Tobin and T. L. Friesz, "Sensitivity analysis for equilibrium network flow," *Transportation Science*, vol. 22, no. 4, pp. 242–250, 1988.
- [19] K. E. Haynes and A. S. Fotheringham, *Gravity and Spatial Interaction Models*, *Scientific Geography*, 2, Sage Publications, California, 1984.
- [20] E. Cascetta, A. Nuzzolo, F. Russo, and A. Vitetta, "A Modified Logit Route Choice Model Overcoming Path Overlapping Problems. Specification and Some Calibration Results for Interurban Networks," in *Proceedings of the 13th International Symposium on Transportation and Traffic Theory*, J. B. Lesort, Ed., Lyon, France, 1996.
- [21] J. G. Wardrop, "Some theoretical aspects of road traffic research," *Proceedings of the ICE*, vol. 1, no. 3, pp. 325–362, 1952.
- [22] H. A. Simon, *A Behavioral Model of Rational Choice*, Wiley, New York, NY, USA, 1957.
- [23] H. A. Simon, *Theories of Decision-Making in Economics and Behavioural Science*, Palgrave Macmillan, London, UK, 1966.
- [24] H. A. Simon, "A mechanism for social selection and successful altruism," *Science*, vol. 250, no. 4988, pp. 1665–1668, 1990.
- [25] H. A. Simon, "Bounded rationality and organizational learning," *Organization Science*, vol. 2, no. 1, pp. 125–134, 1991.
- [26] H. S. Mahmassani and G.-L. Chang, "On boundedly rational user equilibrium in transportation systems," *Transportation Science*, vol. 21, no. 2, pp. 89–99, 1987.
- [27] Y. Lou, Y. Yin, and S. Lawphongpanich, "Robust congestion pricing under boundedly rational user equilibrium," *Transportation Research Part B: Methodological*, vol. 44, no. 1, pp. 15–28, 2010.
- [28] X. Di, H. X. Liu, J.-S. Pang, and X. J. Ban, "Boundedly rational user equilibria (BRUE): mathematical formulation and solution sets," *Transportation Research Part B: Methodological*, vol. 57, pp. 300–313, 2013.
- [29] X. Di and H. X. Liu, "Boundedly rational route choice behavior: a review of models and methodologies," *Transportation Research Part B: Methodological*, vol. 85, pp. 142–179, 2014.
- [30] Y. Sheffi, *Urban Transportation networks: Equilibrium Analysis with Mathematical Programming Methods*, chapters 10 and 11, Prentice-Hall, Inc, USA, 1985.
- [31] Y. Sheffi, *Urban Transportation networks: Equilibrium Analysis with Mathematical Programming Methods*, Prentice-Hall, Inc, Englewood Cliffs, NJ, 1985.
- [32] H. Sbayti, C.-C. Lu, and H. S. Mahmassani, "Efficient implementation of method of successive averages in simulation-based dynamic traffic assignment models for large-scale network applications," *Transportation Research Record: Journal of the Transportation Research Board*, no. 2029, pp. 22–30, 2007.
- [33] G. F. Newell, "A simplified car-following theory: a low-order model," *Transportation Research Part B: Methodological*, vol. 36, no. 3, pp. 195–205, 2002.
- [34] L. Leclercq, J. A. Laval, and E. Chevallier, "The Lagrangian coordinates and what it means for first order traffic flow models," in *Proceedings of the 17th International Symposium on Transportation and Traffic Theory*, R. E. Allsop, M. G. H. Bell, and B. G. Heydecker, Eds., pp. 735–753, London, UK, 2007.
- [35] A. Saltelli, M. Ratto, T. Andres et al., *Global Sensitivity Analysis: The Primer*, John Wiley & Sons, Chichester, England, 2008.
- [36] W. Hoeffding, "A class of statistics with asymptotically normal distribution," *Annals of Mathematical Statistics*, vol. 19, pp. 293–325, 1948.
- [37] B. Efron and C. Stein, "The jackknife estimate of variance," *The Annals of Statistics*, vol. 9, no. 3, pp. 586–596, 1981.
- [38] I. M. Sobol, "Sensitivity estimates for nonlinear mathematical models," *Mathematical Modelling and Computational Experiment*, vol. 1, no. 4, pp. 407–414, 1993.
- [39] T. Homma and A. Saltelli, "Importance measures in global sensitivity analysis of nonlinear models," *Reliability Engineering & System Safety*, vol. 52, no. 1, pp. 1–17, 1996.
- [40] A. Saltelli, P. Annoni, I. Azzini, F. Campolongo, M. Ratto, and S. Tarantola, "Variance based sensitivity analysis of model output. Design and estimator for the total sensitivity index," *Computer Physics Communications*, vol. 181, no. 2, pp. 259–270, 2010.
- [41] O. Roustant, D. Ginsbourger, and Y. Deville, "DiceKriging, DiceOptim: two R packages for the analysis of computer experiments by kriging-based metamodeling and optimization," *Journal of Statistical Software*, vol. 51, no. 1, pp. 1–55, 2012.
- [42] I. M. Sobol, "Global sensitivity indices for nonlinear mathematical models and their Monte Carlo estimates," *Mathematics and Computers in Simulation*, vol. 55, no. 1–3, pp. 271–280, 2001.
- [43] G. Pujol, B. Iooss, and A. Janon, *Sensitivity: Sensitivity Analysis, R package version 1.7*, 2013, <http://CRAN.R-project.org/package=sensitivity>.

